

Assessment of gold potential in stream sediments around the Neoproterozoic Boyo area, Betare-Oya Gold District, Eastern Cameroon

Ndema Mbongué Jean-Lavenir (✉ jndema2012@gmail.com)

University of Buea

Mbua Elvis Ngomba

University of Buea

Emmanuel Eseyá Mengu Junior



University of Buea

Research Article

Keywords: Stream sediment, Boyo area, proximal to the source, distal to the source, low and high silver content

Posted Date: October 6th, 2022

DOI: <https://doi.org/10.21203/rs.3.rs-2125237/v1>

License:   This work is licensed under a Creative Commons Attribution 4.0 International License. [Read Full License](#)

Abstract

Stream sediment geochemical survey was carried out in Boyo area, samples collected and analyzed for major, trace and rare earth elements using ICP-MS method. Minerals present in concentrates include gold, zircon, muscovite. The grain size of gold varies from 0.125 to 1 mm, their shape ranges from sub-angular to angular. Gold grains are of two categories: the first category includes those that are distal to the source, the second category comprises those that are proximal to the source. Fe_2O_3 , Al_2O_3 and SO_3 are dominant major elements in stream sediment, sediments are depleted in Nb and Mo. Gold (8440 to > 10000 ppb) has the highest concentration, the Au/Ag (av.: 14.16) ratio exhibits unusual value greater than the value of the upper lithosphere. Sediments ranged into low Ag (0.062 to 8.47 ppm) and high Ag (20 to 51.3 ppm) content, and all of this suggests that the Boyo gold grains result from two sources or derived by two geological processes; the sulphidation was the dominant mechanism of gold ore deposition. Ag-Au-Bi-Cu constitutes the mineralization factor and the chalcophile elements Ag, Bi and Cu serve as potential pathfinders for Au in the Boyo area. The presence of these elements in the same factor suggests that gold is associated with sulphide minerals. Ag-Hg-W association is related to the hydrothermal alteration of wall rock. The association Ag-Au-Bi-Cu indicates a typical primary mesothermal sulphide \pm gold mineralization paragenesis. The Boyo mature sediments derived from intermediate igneous sources that were deposited in a passive margin environment.

1 Introduction

Gold with the symbol Au is an element of group IB which has an atomic number of 79 and atomic mass of 196.966655 making it one of the higher atomic number elements occurring naturally. The crustal abundance of gold is 0.004 and the metal is positioned between Ag and Rg. The terrestrial abundance of gold (0.005 ppm) is similar to that of platinum (Pt: 0.005 ppm) but, low compared with Cu (50 ppm), Ag (0.07 ppm), and the Au/Ag ratio is equal to 0.07. Gold is a siderophile group elements which displays some characteristics that relate it to chalcophile group elements.

Gold is a precious metal which is mined from Archean to Recent in age deposit types. The large variability in the geological setting of gold deposits suggests its transport and concentration by magmatic, hydrothermal and sedimentary processes. It occurs alongside with platinum-group elements (PGE) and some heavy minerals like magnetite, ilmenite, garnet zircon, rutile, monazite and cassiterite (Frimmel, 2007). Gold combines only with tellurides, selenides and bismuthides (Boyle, 1987; Macdonald, 2007) and alloyed with Ag, Cu, Bi, Hg and PGE. Two types of auriferous deposits that include lode (or vein) deposits and placers are recognized (Boyle, 1987). The enigmatic quartz-pebble conglomerate deposits and the largest auriferous concentrations on earth are classified as modified paleo-placers closely related to lode deposits. Gold is widespread in low concentration in igneous rocks, it also occurs in primary hydrothermal in ore veins, in contact metamorphic deposits, in pegmatites, pyrite, arsenopyrite, quartz and other minerals (Korbel and Novak, 2001). Hydrothermal deposits (veins) associated with quartz and pyrite and placers deposits (Boyle, 1987) that derived from the weathering of gold-bearing rocks contain significant amounts of gold.

In its native state, gold occurs in tellurides and selenides (Boyle, 1987; Macdonald, 2007), and as inclusion in pyrite; it alloyed with Ag, Cu, Bi, Hg, and PGE. ^{197}Au is only the one naturally occurring isotope of gold and the principal oxidation states of Au are + 1 (aurous) and + 3 (auric). Au is mainly present in the following complexes: $[\text{Au}(\text{CN})_2]^-$, $[\text{AuCl}_2]^-$, $[\text{Au}(\text{OH})_4]^-$, $[\text{AuCl}_4]^-$, $[\text{AuS}]$. The most common compounds include AuCl_3 and HAuCl_4 ;

aurostibite and tellurides being the principal ore minerals of Au. Numerous Au and Au-Ag tellurides exist in which sylvanite, calaverite, petzite, krennerite and nagyagite are the most common occurring. Other auriferous compounds include antimonide (AuSb_2), argentiferous gold selenide (Ag_3AuSe_2), uytendogaardtite (Ag_3AuS_2) and bismuthide (Au_2Bi).

Morphological changes in gold particles are attributed to hammering and abrasion (Youngson and Craw, 1999). Little shape modification is attributed to the mass transport of colluvial gold while significant changes are attributed to distance of travel, or time spent in fluvial systems and nature of bedrocks (Youngson and Craw, 1999). The general characteristics of gold grain morphology is indicative of transport distance (Townley et al., 2003).

The gold metal is among the most valued and sought-after commodity, which can be attributed to its malleability, resistance to corrosion and tarnishing and the glitter, makes it ideal for many jewelry purposes. Now, gold is finding industrial uses due to its high resistance to chemical reaction, high conductivity, ductility and its rareness. The radioactive ^{198}Au is used for medical diagnosis and radiation therapy for the treatment of cancer and rheumatoid arthritis (Armendariz et al., 2004; Macdonald, 2007), and as a tracer in industrial applications. Others use of gold include electronics, coins and decorative. Gold alloys are used in industrial applications such as electroplating, granulation, pressing and lamination.

The aim of this study is to investigate the geochemical distribution of gold, to determine the gold grains morphology and to examine the frequency distribution of elements associated with gold in stream sediment from Boyo area, situated within the Pan-African basement in Cameroon where important small-scale alluvial gold mining sites are found.

2 Geologic Setting

The Boyo area lies between longitudes $13^\circ 57' - 13^\circ 59'$ East and between latitude $5^\circ 27' - 5^\circ 30'$ North. It is situated in the Pan-African fold belt (Nzenti et al. 1998; Toteu et al., 2001; 2004) in Cameroon (Fig. 1). The Pan-African fold belt or Central African Orogen is a major Neoproterozoic Orogen linked to the Trans-Saharan Belt of western Africa and to the Brasiliano Orogen of NE Brazil (Castaing et al., 1994, Neves et al., 2006; Fig. 1a). The Pan-African fold belt in Cameroon also called Neoproterozoic fold belt or North-Equatorial fold belt (Poidevin, 1983; Nzenti et al., 1988) is made up of three structural domains (Toteu et al., 2004):

(1) The Yaoundé domain (YD) which corresponds to the northern edge of the Congo Craton is formed by a large Neoproterozoic nappe unit thrust onto the Congo craton towards the south (Fig. 1b). The Oubanguides Nappe in the Republic of Central Africa represents the eastern prolongation or extension of this thrust. The Yaoundé Group comprises Neoproterozoic metasedimentary units including Ntui-Betamba, Mbalmayo-Bengbis-Ayos and Yaoundé Series. This domain includes low- to high-grade metasediments dated at 616 Ma (Ngnotué et al. 2000, Nzenti et al. 1988, Penaye et al. 1993) associated with an alkaline magmatism (Nzenti, 1998) metamorphosed under a medium- to high pressure metamorphism and granulite facies ($750-800^\circ\text{C}$ and $10-12$ kb). The metasediments consist of epicontinental deposits and were deposited to a passive margin (Nzenti et al. 1988) or to an intracontinental distensive environment.

(2) The Adamawa–Yade domain (AYD), which contains the present study area (Fig. 1b) extends east of the Tchollire–Banyo shear zone represents a Paleoproterozoic basement that was dismembered during the Pan-

African. It includes (i) remnants of Paleoproterozoic materials and 2.1 Ga granulitic relict metamorphism that was reworked during Pan-African event, (ii) Neoproterozoic formations from the Lom Serie dated at 700 Ma composed of low- to medium- grade metasediments and volcanoclastic rocks metamorphosed under amphibolite metamorphic facies, and (iii) syn- to late-tectonic granitoids of crustal origin or transitional composition (Toteu et al., 2001). The AYD is also characterized by major NE-striking transcurrent shear zones, regarded as prolongations of the major shear zones of northeast Brazil in a pre-drift Gondwana reconstruction (Castaing et al. 1994). The study area is situated in the Betare-Oya Gold District which lies within the Lom Basin (Soba, 1989; Kankeu et al., 2012). The Lom Basin is a syn-depositional Neoproterozoic pull-apart basin (Ngako et al., 2003) bordered by the Sanaga Fault. The Lom series is well-known for its lode gold mineralization (Ngatcha et al. 2019; Takodjou Wambo et al. 2020).

(3) The Western Cameroon domain (WCD) is located west of the Tcholliré–Banyo shear zone and extends along the western border of Cameroon (Fig. 1b). The WCD consists of (i) Neoproterozoic medium- to high- grade metasediments and metavolcanic rocks of tholeiitic and alkaline affinities dated at about 800 Ma (Toteu et al., 1990); (ii) Pan-African pre, syn-, to late-tectonic granitoids emplaced between 660 and 580 Ma (Toteu et al., 2001); (iii) post-tectonic granitoids; (iv) unmetamorphosed sedimentary and volcanic rocks.

3 Methods Of Investigation

Sampling sites in the study area were located using the Global Positioning System (GPS) and coordinates introduced into a geographic information system (GIS) platform (ArcGIS v. 10.1) to generate a map showing the spatial distribution of the sampling points in the study area. The main river call River Boyo and its tributaries were sampled and panned for gold grain recovery, a total of 15 samples were collected upstream along active stream beds. The sediments were sampled at water depths that vary between 40 and 50 cm.

At each sampling site a pit was dug using a digger down to the gravel layer and 10 kg of active stream sediment was collected into a measuring bucket using a spade and then weighed. The sample was then poured into an aluminum basin and panned to obtain the heavy mineral concentrate. In circular and pendulum motion under water, the panning dish was repeatedly shake and moved in cycles in order to wash-off the light particles and minerals while the heavier minerals were obtained. These concentrates were put in sample bags, coded and taken to the base. They were further spread out on sheets as they were sun dried for four to five days.

In the laboratory, the heavy mineral concentrates collected were subjected to a series of investigations:

- i. Magnetic separation was done to separate magnetic fraction from the non-magnetic fraction.
- ii. The magnetic fraction of the concentrates was examined in order to carry out mineral identification. This was done using the Euromex Eco Blue Polarisation microscope at the Geological Laboratory of the University of Buea.
- iii. Sieve analysis was carried out at the Geological Laboratory of the University of Buea. The concentrate was panned to separate the heavy minerals from the gold grains and the initial weight of the grains taken and recorded. The gold grains were then sieved using the standard granulometry stacked sieve. The various fractions retained on the sieve weighed and recorded with the use of an electronic balance.

iv. Geochemical analysis was done at the Activation Laboratories (ACTLABS), in Canada, for the determination of major, trace and rare earth elements concentration by using Aqua Regia (Total digestion)-Inductively Coupled Plasma-Mass Spectrometry (AR-ICP-MS) method, the procedure as follow:

Argon plasma with working temperature of 6000–8000°C was generated by radio frequency excitation. 10g of prepared solution was fuse with lithium-borate, methaborate and then leached with 30% dilute nitric acid (HNO₃) were injected into the plasma. The solution was excited and produced analyte ions which were separated and measured by mass spectrometry. To test for analytical precision, replicate samples chosen from the batch were randomly in each analysis, the results of replicate analyses and typical detection limits were reported by ACTLABS.

4 Results

4.1 Mineralogy, grain size distribution and morphology of gold grains

A total of 15 samples were collected and the sample location map was produced in which the collected samples are displayed on the drainage map (Fig. 2), all the samples show a lot quantity of gold grains (Fig. 3a). The magnetic fraction of the heavy mineral concentrate has been submitted for petrographic investigation (Fig. 3b) and the minerals present in the concentrate include euhedral, elongated and subrounded to rounded gold grains (40–50%), euhedral and elongated zoning (showing a dark rim and a light core) and unzoned zircon crystals (20–30%) and sheet-like shaped muscovite (5–10%; Fig. 3b).

Results of the grain size analyses show that the gold grains range in size from 0.125 to 1 mm (Table 1; Fig. 4). The grains are predominantly concentrated in the 0.25 mm size grade with a weight of 0.4g followed by 0.5 mm, 1 mm and 0.125 mm size grade with 0.3g wt%, 0.2g wt% and 0.1g wt% respectively. Gold grains recovered from stream sediment in the study area display various shapes and size. They are generally irregular, sub-angular to angular and sub-surrounded to rounded in shape (Fig. 4). The bar chart representation resulting from the grain size distribution of gold grains recovered from the stream sediments of Boyo shows a bell-shaped curve (Fig. 5a) indicating that the gold population exhibits a normal distribution. Their median value (0.3875 mm) is obtained both from the calculation (Table 1) and from the cumulative curves (Fig. 5b).

Table 1
Grain size distribution of gold grains

Grain size (mm)	Weight (g)	Median	F ¹ (%)	ICP ² (%)	DCP ³ (%)
0.125	0.1	0.3	10	10	100
0.25	0.4	0.35	40	50	90
0.5	0.3	0.3	30	80	50
1	0.2	0.6	20	100	20
N	1	0.3875	100		
1) Frequency; 2) Increase cumulative percentage; 3) Decrease cumulative percentage					

4.2 Geochemistry

The geochemical data of stream sediment samples is given in Table 2 in term of major elements, trace elements and rare earth elements (REEs).

Table 2
Chemical composition of stream sediment samples from Boyo

Samples	P2	P3	P4	P5	P8	P9	P11	P12	P14	P15
TiO ₂ (%)	0.10	0,09	0.09	0.11	0.09	0.09	0.08	0.11	0.08	0.08
SO ₃	< 2.50	< 2.50	< 2.50	< 2.50	< 2.50	< 2.50	< 2.50	< 2.50	< 2.50	< 2.50
P ₂ O ₅	0.10	0.11	0.08	0.12	0.06	0.09	0.10	0.12	0.06	0.08
Na ₂ O	0.02	0.02	0.02	0.02	0.02	0.02	0.02	0.02	0.03	0.02
MgO	0.09	0.10	0.07	0.07	0.08	0.07	0.16	0.07	0.04	0.07
Al ₂ O ₃	0.41	0.42	0.29	0.36	0.38	0.28	0.36	0.73	0.21	0.30
K ₂ O	0.05	0.05	0.07	0.03	0.07	0.05	0.07	0.07	0.03	0.05
CaO	0.12	0.11	0.11	0.09	0.13	0.10	0.11	0.17	0.05	0.09
Fe ₂ O ₃	1.69	1.83	1.26	1.52	1.64	1.22	1.30	1.08	2.25	1.19
Fe ₂ O ₃ * + MgO	1.78	1.93	1.33	1.60	1.72	1.28	1.46	1.14	2.29	1.26
K ₂ O/Na ₂ O	2.40	2.58	4.07	1.72	3.440	3.05	3.44	3.73	1.12	3.05
Al ₂ O ₃ /(CaO + Na ₂ O)	2.90	3.35	2.31	3.43	2.58	2.37	2.85	3.86	2.66	2.71
Ag (ppm)	32.7	40.8	8.47	46.1	4.13	0.062	48.2	51.3	20	47.7
As	< 0.1	< 0.1	< 0.1	< 0.1	< 0.1	< 0.1	< 0.1	< 0.1	< 0.1	< 0.1
Au (ppb)	> 10000	> 10000	> 10000	> 10000	> 10000	8440	> 10000	> 10000	> 10000	> 10000
Au (ppm)	> 10	> 10	> 10	> 10	> 10	8.44	> 10	> 10	> 10	> 10
B	1	1	2	2	2	2	2	2	1	1
Ba	50.8	45.5	42.4	41.6	43.4	37.4	40.6	56.5	36.2	38.1
Be	0.5	0.5	0.6	0.7	0.5	0.6	0.4	0.5	0.8	0.9
Bi	0.44	0.38	0.32	0.45	0.35	0.3	0.38	0.32	0.41	0.36
Co	5.1	5.4	3.2	4.2	4,1	3,3	3.4	7.3	2.6	3.4
Cr	25	25	20	23	23	18	18	34	17	20
Cs	0.22	0.19	0.2	0.16	0.24	0.18	0.21	0.25	0.12	0.14
Cu	8.9	9	9.1	10.1	11.3	0.4	6.4	9	3.1	5.7
Ga	0.1	0.43	< 0.02	0.73	< 0.02	< 0.02	< 0.02	1.4	< 0.02	< 0.02

Samples	P2	P3	P4	P5	P8	P9	P11	P12	P14	P15
Ge	<0.1	<0.1	<0.1	<0.1	<0.1	<0.1	<0.1	<0.1	<0.1	<0.1
Hf	0.4	0.3	0.4	0.3	0.4	0.3	0.3	0.3	0.3	0.4

Table 2
Continued 1

Samples	P2	P3	P4	P5	P8	P9	P11	P12	P14	P15
Hg (ppb)	80	140	40	230	180	60	480	370	300	560
In	0.03	0.03	0.03	0.04	0.03	0.03	<0.02	<0.02	0.04	0.03
Li	1.4	1.3	1.3	1.1	1.5	1.2	1.4	1.9	0.8	1
Mn	322	302	295	311	331	293	288	350	250	263
Mo	0.16	0.14	0.09	0.06	0.17	0.09	0.09	0.21	0.03	0.09
Nb	1.1	0.9	1	0.6	1	1	1.1	1.6	0.4	0.7
Ni	39.4	27.7	26.1	12.6	19.2	12.9	11.8	21.5	9.8	8.1
Pb	25.3	21.3	21.8	23.1	22.4	23.9	21.9	20.5	21.7	19.6
Rb	2	1.8	2.2	1.5	2.3	2.1	2.3	2.6	1.1	1.4
Re	0.002	0.002	0.002	0,001	0.002	0.001	0.001	0.002	0.001	0.001
Sb	0.43	0.28	0.11	0.16	0.14	0.11	0.13	0.11	0.13	0.11
Sc	3.1	5.5	4.5	6.8	3.1	5.3	2.6	3.3	9.7	10.4
Se	<0.1	<0.1	<0.1	<0.1	<0.1	<0.1	<0.1	<0.1	<0.1	<0.1
Sn	1.12	0.9	0.97	0.91	1.01	0.88	0.96	0.88	0.92	0.81
Sr	10.9	10.5	10.1	9.3	11.4	9.5	10.7	15.9	6.5	9.7
Ta	<0.05	<0.05	<0.05	<0.05	<0.05	<0.05	<0.05	<0.05	<0.05	<0.05
Te	0.04	0.05	<0.02	<0.02	0.04	<0.02	0.02	0.04	0.04	0.05
Th	>200	>200	>200	186	>200	>200	>200	>200	>200	>200
Tl	0.03	0.05	0.03	0.03	0.06	0.04	0.04	0.04	0.04	0.03
U	35.7	27.8	37.2	20.8	37.7	30.4	30.7	27.4	24.1	28.8
V	37	38	31	31	35	32	29	48	29	34
W	0.2	0.1	<0.1	<0.1	0.1	<0.1	0.2	0.2	<0.1	0,4
Y	80	80.7	93.4	76.9	86.1	85.8	69.8	67.5	96.5	117
Zn	29,9	26.2	21.6	31.6	25.1	22.2	21.7	31.3	22.4	23.2
Zr	4.2	3.5	4.1	3.5	4.5	3.6	4.5	5.6	2.3	3.3
As x 100	10	10	10	10	10	10	10	10	10	10
Cu x 100	890	900	910	1010	1130	40	640	900	310	570

Table 2
Continued 1

Samples	P2	P3	P4	P5	P8	P9	P11	P12	P14	P15
Hg (ppb)	80	140	40	230	180	60	480	370	300	560
In	0.03	0.03	0.03	0.04	0.03	0.03	<0.02	<0.02	0.04	0.03
Li	1.4	1.3	1.3	1.1	1.5	1.2	1.4	1.9	0.8	1
Mn	322	302	295	311	331	293	288	350	250	263
Mo	0.16	0.14	0.09	0.06	0.17	0.09	0.09	0.21	0.03	0.09
Nb	1.1	0.9	1	0.6	1	1	1.1	1.6	0.4	0.7
Ni	39.4	27.7	26.1	12.6	19.2	12.9	11.8	21.5	9.8	8.1
Pb	25.3	21.3	21.8	23.1	22.4	23.9	21.9	20.5	21.7	19.6
Rb	2	1.8	2.2	1.5	2.3	2.1	2.3	2.6	1.1	1.4
Re	0.002	0.002	0.002	0,001	0.002	0.001	0.001	0.002	0.001	0.001
Sb	0.43	0.28	0.11	0.16	0.14	0.11	0.13	0.11	0.13	0.11
Sc	3.1	5.5	4.5	6.8	3.1	5.3	2.6	3.3	9.7	10.4
Se	<0.1	<0.1	<0.1	<0.1	<0.1	<0.1	<0.1	<0.1	<0.1	<0.1
Sn	1.12	0.9	0.97	0.91	1.01	0.88	0.96	0.88	0.92	0.81
Sr	10.9	10.5	10.1	9.3	11.4	9.5	10.7	15.9	6.5	9.7
Ta	<0.05	<0.05	<0.05	<0.05	<0.05	<0.05	<0.05	<0.05	<0.05	<0.05
Te	0.04	0.05	<0.02	<0.02	0.04	<0.02	0.02	0.04	0.04	0.05
Th	>200	>200	>200	186	>200	>200	>200	>200	>200	>200
Tl	0.03	0.05	0.03	0.03	0.06	0.04	0.04	0.04	0.04	0.03
U	35.7	27.8	37.2	20.8	37.7	30.4	30.7	27.4	24.1	28.8
V	37	38	31	31	35	32	29	48	29	34
W	0.2	0.1	<0.1	<0.1	0.1	<0.1	0.2	0.2	<0.1	0,4
Y	80	80.7	93.4	76.9	86.1	85.8	69.8	67.5	96.5	117
Zn	29,9	26.2	21.6	31.6	25.1	22.2	21.7	31.3	22.4	23.2
Zr	4.2	3.5	4.1	3.5	4.5	3.6	4.5	5.6	2.3	3.3
As x 100	10	10	10	10	10	10	10	10	10	10
Cu x 100	890	900	910	1010	1130	40	640	900	310	570

4.2.1 Major elements

The major element composition of stream sediments presented in Table 2 shows that Fe_2O_3 (1.08–2.25%) has the highest concentration with the mean value of 1.49% followed by Al_2O_3 (0.21–0.73%; Fig. 5a). Na_2O (0.02–0.03%) and SO_3 (<2.5%) display constant values (Table 3.2). The rest of the major oxides (CaO : 0.05–0.17%, P_2O_5 : 0.06–0.12%, TiO_2 : 0.08–0.11%, MgO : 0.04–0.16% and K_2O : 0.03–0.07%) exhibit low to very low content (Table 2; Fig. 6a). The enrichment-depletion diagram is presented in Fig. 6b in which the stream sediment samples show depletion in all the major elements, except in SO_3 and Fe_2O_3 .

4.2.2 Trace elements

According to Table 2, the concentration of gold varies from 8440 to > 10000 ppb, that is 8.44 to > 10 ppm according to the relation $1 \text{ ppm} = 10^3 \text{ ppb}$. The average content of gold (9844 ppb or 9.84 ppm) in the studied samples is widely greater than the one of the recommended value of the upper continental crust (Au: 1.5 ppm) after Rudnick and Gao (2003) and also greater to the abundance of gold estimated in the continental crust (Au: 0.004 ppm) according to William (2016). Other trace elements with high concentrations include transition metals such as Mn (250–350 ppm; av. = 300.5 ppm), Hg (40–560 ppb, av.: 244 ppb), Ag (0.062–51.3 ppm; av.: 29.94 ppm), Ni (8. – 39.4 ppm; av. :18.91 ppm), Y (67.5–117 ppm), and Th (186 - > 200 ppm). The studied samples are depleted in high field strength elements (HFSE) such as Zr (2.3–5.6 ppm), Hf (0.3–0.4 ppm), Nb (0.4–1.6 ppm), Ta < 0.05 ppm) and enriched in large ion lithophile elements (LILE) like Sr (6.5–15.9 ppm), Rb (1.1–2.6 ppm), Ba (36.2–56.5 ppm), Pb (19.6–25.3 ppm), Ce (794–1300 ppm), Eu (2.7–4.2 ppm). In the enrichment-depletion plot (Fig. 6b), stream sediments show depletion in Nb and Mo, and enrichment for the rest of trace elements. The composition of stream sediment samples from Boyo were plotted in Au-Ag-As x 100 and Au-Ag-Hg x 25 ternary plots (Fig. 7a, 7b). The plots show very low contents of As (< 1 ppm) and moderate to high concentration of Hg (40 to 560 ppb). Also, As contents are below the detection limit for all the samples (Table 2).

The Table 3 presents the descriptive statistics of elements in stream sediments; skewness and kurtosis coefficients of data for Ag, Hg, U show negative values. Kurtosis coefficients of data for Au (10), Cr (2.58), Ga (3.62), Sb (4.27), Sr (3.85), V (3.19) and W (4.19) are considerably higher when compared to those of other elements. Ni (2.14) and Sc (3.16) show slightly high skewness coefficients (Table 3). The skewness values and the average geometric mean (GM) of elements indicate a symmetric data distribution pattern (Table 3). This is in accordance with the frequency distribution diagrams in which the selected trace elements (Ag, Au, Ba, Cr, Mn, Sr) show a normal and symmetric distribution (Fig. 8). The standard deviation values were high for Ag (20.03), Au (493.32), Hg (108.14), Mn (30.10) and Y (14.43; Table 3). The coefficient of variation (CV) values are greater to 50% for Ag, Cd, Ga, Hg, Ni, Sb, Sc W and smaller than 50% for the rest of the other elements.

Table 3
Basic statistical parameters for stream sediment geochemical data obtained from Boyo

Elements	Min	Mean	Max	Median	GM ¹	CV ² (%)	Std Dev ³	S ⁴	K ⁵
Ag	0.06	29.95	51.3	36.75	14.12	66.88	20.03	-0.48	-1.67
Au	8440	9844	10000	10000	9831.83	5.01	493.32	1.14	10
B	1	1.6	2	2	1.52	32.27	0.52	0.87	-2.28
Ba	36.2	43.25	56.5	42	42.86	14.59	6.31	0.26	0.95
Be	0.4	0.6	0.9	0.55	0.58	26.06	0.16	0.77	-0.03
Bi	0.3	0.371	0.45	0.37	0.37	13.77	0.05	1.3	-1.04
Cd	0.01	0.05	0.11	0.05	0.04	56.57	0.03	1.43	1.35
Co	2.6	4.2	7.3	3.75	4.02	33.22	1.40	-0.31	1.66
Cr	17	22.3	34	21.5	21.85	22.58	5.03	-1.07	2.58
Cs	0.12	0.19	0.25	0.195	0.19	22	0.04	1.98	-0.71
Cu	0.4	7.3	11.3	8,95	5.66	46.58	3.4	0.48	0.46
Ga	0.02	0.28	1.4	0.02	0.07	166.03	0.46	0.63	3.62
Hf	0.3	0.34	0.4	0.3	0.34	15.19	0.05	0.46	-2.28
Hg	40	244	560	205	178.70	73.83	180.14	-0.12	-0.80
In	0.02	0.03	0.04	0,03	0.03	22.22	0.01	0.37	0.08
Li	0.8	1.29	1.9	1.3	1.26	23.24	0.30	0.34	1.25
Mn	250	300.5	350	298.5	299.12	10.02	30.10	0.98	-0.19
Mo	0.03	0.11	0.21	0.09	0.10	48.84	0.06	0.49	-0.55
Nb	0.4	0.94	1.6	1	0.88	34.82	0.33	-0.5	1.23
Ni	8.1	18.91	39.4	16.05	16.80	52.35	9.90	2.14	0.46
Pb	19.6	22.15	25.3	21.85	22.10	7.42	1.64	0.95	0.42
Rb	1.1	1.93	2.6	2.05	1.87	24.43	0.47	0.96	-0.66
Re	0.001	0.002	0.002	0.0015	0.001	35.14	0.00	1.06	-2.57
Sb	0.11	0.17	0.43	0.13	0.15	61.11	0.10	-0.13	4.27
Sc	2.6	5.43	10,4	4.9	4.86	51.03	2.77	-3.16	-0.30
Sn	0.81	0.94	1.12	0.915	0.93	9.11	0.09	-0.04	1.65
Sr	6.5	10.45	15.9	10.3	10.22	22.42	2.34	1.63	3.85

1) Geometric mean; 2) Coefficient of variation; 3) Standard deviation; 4) Skweness; 5) kurtosis

Elements	Min	Mean	Max	Median	GM ¹	CV ² (%)	Std Dev ³	S ⁴	K ⁵
Te	0.02	0.03	0.05	0.04	0.03	37.2	0.01	1.07	-1.87
Th	186	198.6	200	200	198.55	2.23	4.43	0.65	10
Tl	0.03	0.04	0.06	0.04	0.04	25.5	0.01	0.14	0.91
U	20.8	30.06	37.7	29.6	29.59	18.45	5.55	-0.04	-0.71
V	29	34.4	48	33	34.02	16.57	5.70	1.63	3.19
W	0.1	0.16	0.4	0.1	0.14	60.38	0.10	1.96	4.19
Y	67.5	85.37	117	83.25	84.35	16.9	14.43	1.07	1.64
Zn	21.6	25.52	31.6	24.15	25.25	15.8	4.03	0.65	-1.41
Zr	2.3	3.91	5.6	3.85	3.82	22.67	0.89	0.14	1.08

1) Geometric mean; 2) Coefficient of variation; 3) Standard deviation; 4) Skewness; 5) kurtosis

4.2.3 Rare earth elements

The total REE values range from 1684.9 to 2382.8 ppm. The average concentration of REE in this study is higher (2270.17 ppm) compared with the values from the upper continental crust (REE: 10.45 ppm after Taylor and McLennan, 1985; 1995), (REE: 10.77 ppm; according to Wedespohl, 1995) and (REE: 10.58 ppm after Rudnick and Gao, 2003). Therefore, the REE contents in this study are about 214 times the values of the upper continental crust (UCC). Upper continental crust normalized REE patterns (Fig. 9) are strongly fractionated ($La_N/Yb_N = 2.96-12.31$) with light rare earth elements (LREE) enrichment ($La_N/Sm_N = 1.06-1.24$) compared to the heavy rare earth elements (HREE): $Gd_N/Yb_N = 2.20-9.29$), and a negative Eu anomaly ($Eu/Eu^* = 0.24-0.31$).

4.3 Multivariate statistical analysis (MSA)

4.3.1 Pearson's correlation coefficient factor

The correlation coefficient values of the elements, using Pearson's correlation method for the studied stream sediment samples is given in Fig. 10. In this figure, the strong correlation coefficient values ($r = 0.70-0.99$) are represented with the yellow colour, moderate correlation coefficient values ($r = 0.50-0.69$) show red colour and very strong correlation coefficient values ($r = 0.80-0.99$) are in green. Au exhibits a strong positive correlation with Cu ($r = 0.71$) and a moderate correlation with Ag ($r = 0.52$). The values of Ag increase with the values of Al_2O_3 ($r = 0.59$), P_2O_5 ($r = 0.67$), W ($r = 0.55$), while the concentration of Bi decreases with the values of Nb ($r = -0.50$), Rb ($r = -0.56$) and Th ($r = -0.54$; Fig. 10).

4.3.2 Factor analysis

The eigenvalues, the percentage of the variance and the cumulative percentage have been determined in accordance with the factors. The scree plot (Fig. 11) shows the calculated eigenvalues arranged from the largest values to the smallest values. The plot shows a steep slope toward the seventh factor and displays a constant gentle slope. The highest eigenvalue which is 15.002 is related to the first component with variability percentage of 24.907% (Table 4). The varimax rotation method is applied to the coefficient factors; seven element

associations represented by factors 1 to factor 7 accounting for 34.511% of the variance (eigenvalue) and cumulatively accounting for 95.804% of the total data variance were identified according to Table 4. Factor 1 (F1) contains the transitional metals and lithophile elements: Ba, Co, Cr, Ga, Mn, Li, Mo, Re, Sr, V, Zn, Zr and accounts for 24.907% (Table 4). The trace element content of this factor points to the presence of granitic rocks and thus constitutes a lithologic control. These elements are probably produced by the weathering of the basement rock in the study area. The variability of the elements in factor 1 indicates these elements have been controlled by the mixed rock types occurring in the area. The Zr present in this factor is explained by the presence of zircon and confirm the afore mentioned result. Factor 2 (F2) unites three lithophile elements Hf, U and Y that represents 18.421%. Factor 3 (F3) includes Bi, Ni, Pb, Sb and Sn; it accounts for 12.074%. Factor 4 (F4) accounts for 8.093% and it loaded by Te and Th. Factor 5 (F5) displays an association between chalcophile elements such as Ag, Au, Bi, Cu and accounts for 7.112%. Factor 6 (F6) is strongly loaded by transitional metals and lithophile elements: B, Cs, Li, Mn, Mo, Nb, Rb, Sr, U, Zr; it accounts for 27,007%. The trace element content of this factor also points to the presence of granitic rocks. Factor 7 (F7) consists of Ag, Hg, W that contribute for 8,191% of total variance.

Table 4
Eigenvalues, percentage of the variance, and cumulative percentage of variance in accordance with the calculated factors for stream sediments from Boyo.

Variable	F1	F2	F3	F4	F5	F6	F7
Ag	0.368	-0.420	-0.065	-0.024	0.414	-0.052	0.680
Au	0.172	0.080	0.040	0.106	0.861	-0.063	0.195
B	-0.005	-0.027	-0.350	-0.606	-0.117	0.653	-0.264
Ba	0.841	0.008	0.271	0.077	0.145	0.399	0.081
Be	-0.154	0.243	-0.352	-0.111	-0.092	-0.839	0.249
Bi	-0.073	-0.289	0.572	-0.222	0.538	-0.439	0.185
Cd	0.025	-0.388	-0.013	0.189	-0.024	-0.815	0.222
Co	0.928	-0.167	0.103	0.113	0.098	0.272	0.051
Cr	0.959	-0.041	0.025	0.034	0.156	0.228	0.024
Cs	0.453	0.134	0.166	0.063	0.100	0.840	-0.155
Cu	0.439	0.263	0.139	-0.178	0.773	0.255	-0.157
Ga	0.856	-0.360	-0.216	-0.233	0.082	0.081	0.050
Hf	-0.070	0.944	0.188	0.091	0.203	0.051	0.130
Hg	-0.074	-0.240	-0.533	0.157	0.305	-0.031	0.680
In	-0.214	0.047	0.155	-0.312	0.088	-0.833	-0.348
Li	0.621	0.018	0.005	0.059	0.049	0.778	-0.032
Mn	0.719	0.062	0.184	-0.199	0.109	0.555	-0.219
Mo	0.724	0.181	0.117	0.305	0.076	0.534	-0.052
Nb	0.549	0.043	0.021	0.111	-0.188	0.795	0.112
Ni	0.427	0.283	0.725	0.177	0.080	0.239	-0.149
Pb	-0.119	-0.004	0.812	-0.335	-0.273	0.107	-0.231
Rb	0.309	0.108	-0.010	0.000	-0.129	0.930	-0.108
Re	0.558	0.386	0.288	0.294	0.229	0.356	-0.355
Sb	0.234	0.017	0.909	0.206	0.147	-0.087	0.066
Sc	-0.199	0.029	-0.350	0.058	-0.048	-0.888	0.205
Sn	-0.075	0.219	0.800	-0.019	0.237	0.338	-0.183
Sr	0.741	0.043	-0.134	0.055	0.036	0.638	0.139
Te	0.403	0.136	-0.022	0.734	0.272	-0.376	0.106

Variable	F1	F2	F3	F4	F5	F6	F7
Th	-0.109	0.241	-0.022	0.833	-0.265	0.314	0.033
Tl	0.039	-0.117	-0.168	0.411	0.148	0.278	-0.559
U	-0.154	0.695	0.271	0.263	-0.031	0.571	-0.155
V	0.933	0.011	-0.055	0.270	-0.036	0.219	0.068
W	0.077	0.264	-0.206	0.221	0.045	-0.070	0.889
Y	-0.341	0.590	-0.284	0.228	-0.084	-0.602	0.184
Zn	0.810	-0.167	0.303	-0.347	0.236	-0.068	0.072
Zr	0.516	0.095	-0.044	-0.075	0.070	0.835	0.108
Eigenvalue	15.002	5.859	4.620	3.871	2.072	1.706	1.380
Variability (%)	24.907	8.421	12.074	8.093	7.112	27.007	8.191
Cumulative %	24.907	33.328	45.402	53.494	60.607	87.613	95.804

4.3.3 Cluster analysis

The result of cluster analysis is shown in the hierarchical clustering diagram or dendrogram (Fig. 12). The Dendrogram (Fig. 12) shows two main clusters with three sub-clusters: cluster I is made up of 4 parageneses that include: (i) Ag-Hg-W-Te, (ii) Be-Sc-Y, Be, (iii) Bi-In and (iv) Cd-Na₂O-Fe₂O₃. Cluster II is composed of (v) Au-Cu, (vi) Ba-Co-Cr-Al₂O₃-V, (vii) Ga-Zn-TiO₂, (viii) B-MgO, (ix) Cs-Rb, (x) Li-Zr-Nb, (xi) Sr-CaO, (xii) Mn-Mo, (xiii) 13: Hf-U, (iv) Ni-Re, (xv) Pb-Sn-Sb and (xvi) Th-K₂O-Tl parageneses. A notable feature of the Boyo stream sediment is the association Au-Cu (Fig. 12).

5 Discussion

5.1 Morphological evolution of gold particles and gold variation in stream sediments

Gold is a malleable native element whose morphological feature evolve more rapidly than silicates in response to physical weathering. The transport of gold in fluvial environment depends of the grain size, and the shape. The Boyo gold grains range from 0.125 to 1 mm in size (Fig. 4) and indicate a mix population with various degrees of hammering, abrasion and transportation distance. They display various outlines and morphologies confirming evolution in a fluvial environment similar to those described in Otago in New Zealand (Youngson and Craw, 1999) and in Southern Cordillera in Chile (Townley et al., 2003). Based on the morphological characterization of gold grains by Townley et al. (2003), the Boyo alluvial gold grains are of two categories. The first category (Fig. 4a, 4b) comprises Au grains that are distal to the source (50 to more than 300 m), they are rounded and sub-rounded with irregular outline, irregular topography, branched and bent-up to folded outlines, and pitted surfaces and cavities due to hammering and abrasion. The second category (Fig. 4c, 4d) includes Au grains that are proximal to the source (0–50 m), they appear oblong with angular and sub-angular edges, and regular shape. These grains experienced little attrition and deformation in the fluvial system. They are uniformly distributed,

contrasting the result of Embui et al. (2013). In the study area, there is no significant variation between the Au concentrations obtained from panning and geochemical exploration). A challenge faced in stream sediment geochemical survey is that of an erratic distribution of gold in the different size fractions of sediments (Chandrajith et al., 2001). Given that the Au determined from panning and weighing method corroborate that from geochemistry and allows the use of any size fraction for exploration in the study area. According to Bellehemeur et al. (1994), Garrett et al. (2004) and Mimbo et al. (2004), Au concentrations in stream sediments is usually very low (< 1 ppb) or below the detection limit. This study however, shows high Au concentration of > 10000 ppb (Table 2). Because stream sediments represent materials weathered from parent rock transported downstream, the mineral content of stream sediments depends on the primary mineral of the rock, the degree of weathering and the dispersion mechanism (Ali et al., 2006; McClenaghan and Cabri, 2011).

5.2 Element associations and spatial distribution

From the correlation analysis (Fig. 10), Au shows high correlation only with Cu ($r = 0.71$) and moderate correlation with Ag ($r = 0.52$). Other element pairs exhibit positive correlation with their respective correspondents. The correlation coefficients of selected elements have been plotted in Fig. 13, the similarity in the patterns for Ag and Cu (Fig. 13) implies some geochemical coherence and suggests similar input sources and common geochemical characteristics of the elements. Therefore, trace element concentrations in stream sediments of Boyo were of geogenic origins. Meanwhile, the Boyo stream sediments are subdivided into two groups: the first group with low Ag values (Ag: 0.062–8.47 ppm, av. = 4.22 ppm) and the second group comprises high Ag contents (Ag: 20–51.3 ppm, av. = 25.73 ppm; Table 2). All this suggests that the Boyo gold grains result from two sources or derived by two geological processes in which the sulphidation was the dominant mechanism of gold ore deposition. The factor 5 which is made up of chalcophile elements (Ag, Au, Bi, Cu) constitutes the mineralization factor and the presence of these elements in the same factor suggests that gold is associated with sulphide minerals. The association Ag-Au-Bi-Cu indicates a distinctive primary mesothermal sulphide \pm Au mineralization paragenesis (Pirajno, 1992; Embui et al., 2013). Artisanal gold exploration has been carried out in Boyo area and the on-going artisanal gold mining supports the placer gold mineralization. The evidence of placer gold mineralization in Boyo is also supported by the presence of free gold grains in the panning and weighing method. Elements of factor 7 (Ag, Hg, W) do not have any relationship with Au and the association Ag-Hg-W also represents a sulphidation event. According to Embui et al. (2013), this type of association is attributed to the hydrothermal alteration of wall rock. Elements with similar behaviors were determined with cluster analysis (Fig. 12) and categorized in groups (cluster I and cluster II). Therefore, the conformity between Au obtained from panning method with geochemistry points to Cu as being the only element that Au associates (Fig. 12) in the study area. The Au-Cu paragenesis recorded in Boyo area should be compared with the porphyry Cu (\pm Au) paragenesis (Boyle, 1984; McQueen, 2005; Rodionov et al., 2013). The Au/Ag (0.19–136.13, av. = 14.16) ratio in the studied stream sediment is variable and exhibit unusual values largely greater than the Au/Ag ratio (0.1) in the upper lithosphere (Boyle, 1984), with sample P9 showing the high ratio (Au/Ag = 136.13). The stream sediment samples show elevated content in REEs (1684.9–2382.8 ppm, av. = 2270.17 ppm) notably in LREEs (53–1300 ppm, av. = 433.62 ppm), this may be to the presence of REE-bearing mineral such as monazite, and the negative Eu anomaly could be due to the presence of feldspar (plagioclase).

The distribution of Au in the study area is regular (Fig. 2), the River Boy and tributaries show a lot quantity of gold in the pan concentrate (Fig. 5.2). The distribution maps for elements of factor 5 have generated (Fig. 14). The concentrations of the selected elements exhibit considerable variation in space distribution, Au has the highest

concentrations and shows a geographic trend (Fig. 14). The spatial distribution of Au and associated chalcophile elements such as Ag, Bi and Cu is sporadic with no clear pattern along the drainage system (Fig. 14). These chalcophile elements show low concentration and serve as potential pathfinders for Au in the study area. They also show moderate to strong correlation and spatial association with Au. The coefficient of variation (CV) values of Boyo ranged into two groups: (i) the low CV values range from 2.23–48.84% (Table 3) and correspond after Karanlik et al. (2011) to a spatially homogeneous distribution of element concentrations; the majority of the analyzed elements (27 elements) fall within this group. (ii) Elements with the high CV (51.03–166.03%) values (Table 3) include Ag, Cd, Ga, Hg, Ni, Sb, Sc W indicate a non-homogenous surface distribution. This observation is also confirmed with the standard deviation values. The low standard deviation values ($\leq 30.10\%$; Table 3) suggest a spatially homogeneous distribution. Au (433.33%) and Hg (180.14%) show elevated standard deviation values suggesting a non-homogenous surface distribution and a high variability for these elements. The very low positive skewness values suggest that individual trace elements were very weakly right-skewed and, the very low negative kurtosis values indicate a very slightly light-tailed distribution. All this result is confirmed with the bar chart graphs in which histograms of original data distribution of elements show symmetric and normal distribution (Fig. 8).

5.3 Source of provenance, sediment maturity, weathering and tectonic environment

In this study, we used the discriminant function diagram of Roser and Korsch (1988) to infer the source of provenance of the Boyo stream sediment (Fig. 15a). In this diagram (Fig. 15a), all the stream sediment samples from Boyo yield intermediate igneous provenance suggesting that the alluvial gold from Boyo area proven from intermediate igneous rocks. The sediment provenance of the studied area can be compared with the sediment provenance from Mbiame floodplain (Etutu et al., 2020). The Boyo stream sediments exhibit high Th/Sc (av.: 45.23) and La/Sc (av.: 121.55; Table 2) ratios, which are greater than those of the recommended values of UCC (Th/Sc = 0.75 and La/Sc = 2.21; Rudnick and Gao, 2003) and closer to sediments from mixed felsic/basic source). This indicates that the studied sediments originated from a mixed felsic/basic source, and in the La/Th vs. Hf diagram (Fig. 14b), all the studied samples cluster within the mixed felsic/basic source field.

The source characteristics of sediments is constrained with the Sr vs. Ba plot (Fig. 15c) by (Floyd et al., 1989) in which the Boyo sediments plots within the field of mature sediments (Fig. 15c). The maturity of these sediments is also confirmed with the moderate Zr–Hf content since Hf and Zr are closely associated in sediments and are both concentrated in zircon. Ndema Mbongué and Mbonjoh (2020) also recorded mature sediment as source characteristic of sediments for the Gouap banded iron formations. This result is different with the studies of Moudioh et al. (2020), Chombong et al. (2013) and (Soh Tamehe et al. 2018).

The detrital fraction of the studied sediments is constrained by La/La* versus Yb discrimination diagram after Jahn and Condie (1995). In this diagram the Boyo stream sediment samples plotted onto the detritus field (Fig. 15d) suggesting a detritus-free mineralization. This result is also supported by Ni (81–39.4 ppm), V (29–48 ppm) and Sc (2.6–10.4 ppm) contents in stream sediments suggesting after Yang et al. (2014) clastic and detritus inputs. Meanwhile, low concentrations of Al₂O₃ (0.21–0.73%), TiO₂ (0.08–0.11%), Na₂O (0.02–0.03%), K₂O (0.03–0.07%) and the correlation between Na₂O and K₂O ($r = -0.54$) suggest some sources of contamination. The Boyo stream sediments display high La (383–1300 ppm) contents reflecting felsic input. Therefore, the La-Th-Sc ternary plot by Bhatia and Crook (1986) was used to determine the source of

contamination of the Boyo sediments. Boyo stream sediment samples fall within the field of granitic gneiss sources (Fig. 15e). This indicates that the source of detrital contamination in the Boyo stream sediment resulted from granitic gneiss. Furthermore, since Th/U ratio (> 4.0) in sedimentary rocks reflect important weathering at the primary source (McLennan et al., 1993), the high Th/U ratios (5.31–8.94; av. : 6.81) recorded in the studied area compared with the value of UCC (Th/U = 3.89 after Rudnick and Gao (2003) and Th/U = 3.82 according to Taylor and McLennan, 1985; 1995) indicate these sediments have undergone weathering as shown by the Th/U vs. Th diagram (Fig. 15f).

Maynard et al. (1982), Bhatia (1983), Bhatia and Crook (1986), Roser and Korsch (1986) and Kroonenberg (1994) related sediments geochemistry to specific tectonic environment. The inter trace elements in clastic sediments have also been used in discrimination diagrams of plate tectonic settings (Varga and Szakmany, 2004), these elements can be transferred quantitatively into detrital sediments during weathering and transportation to reflect the signature of the parent material (Armstrong-Altrin et al., 2004). For this study, the discrimination diagrams of tectonic settings after Bhatia (1983) and Roser and Korsch (1986) were used to evaluate the tectonic setting of the Boyo stream sediment samples. In these diagrams (Fig. 16a to 16d), samples cluster near the field of passive margin (PM) setting. The Passive Margin setting is also retained for the tectonic setting of the Ntem metasediments (Moudioh et al., 2020).

6 Conclusion

Stream sediment geochemical survey was carried out in the Boyo area situated within the Neoproterozoic or the Pan-African Fold Belt in Cameroon. The minerals present in the heavy mineral concentrate include gold, zircon and muscovite. Gold grains were identified both in the pan concentrate and under the microscope, their grain size varies from 0.125 to 1 mm and the shapes of the gold grains ranged from sub-angular to angular. They display various outlines and morphologies which confirms evolution in a fluvial environment. The Boyo alluvial gold grains are of two categories indicating a mix population with various degrees of hammering, abrasion and transportation distance. The first category includes those that are proximal to the source and appear oblong with angular and sub-angular edges, and regular shape. These grains experienced little attrition and deformation in the fluvial system. The second category comprises those that are distal to the source, they are rounded and sub-rounded with irregular outline, irregular topography, branched and bent-up to folded outlines, and pitted surfaces and cavities due to hammering and abrasion.

The chemical analysis of the Boyo stream sediment has revealed that Fe_2O_3 , Al_2O_3 and SO_3 are the dominant major elements, the sediments are depleted in Nb and Mo and enriched for the rest of trace elements. Gold has the highest concentrations followed by Mn, Hg, Th, Y and the Au/Ag ratio exhibit unusual values largely greater than the value of the upper lithosphere. Upper Continental Crust normalized REE patterns shows LREE enrichment compared to the HREE, and a negative Eu anomaly. The frequency distribution graphs show a normal and symmetric distribution, and the spatial variability of trace elements and the low coefficient of variation values were in accordance with a spatially homogeneous distribution.

Correlations between elements and the correlation coefficients patterns for Ag and Cu suggests some geochemical coherence and evidence for similar input sources and common geochemical characteristics of elements. Trace element concentrations in stream sediments of Boyo were of geogenic origins. Meanwhile, Boyo stream sediments ranged into two groups including low Ag content and high Ag contents, and all of this

suggests that the Boyo gold grains result from two sources or derived by two geological processes and, the sulphidation was the dominant mechanism of gold ore deposition.

Multi-element statistical analysis shows a strong association of Au with the chalcophile elements Ag, Bi, Cu suggesting that gold is associated with sulphide minerals. Ag-Au-Bi-Cu constitutes the mineralization factor and the chalcophile elements Ag, Bi and Cu serve as potential pathfinders for Au in the Boyo area. The paragenesis Au-Ag-Bi-Cu indicates a typical primary mesothermal sulphide ± gold mineralization paragenesis and the development of Ag-Hg-W association is related to the hydrothermal alteration of wall rock.

The Boyo sediment derived from intermediate igneous provenance, these mature sediments that were deposited in a passive margin environment exhibit high Th/Sc and La/Sc compatible with mixed felsic/basic source sediments. The detrital fraction and the source of contamination resulted from granitic gneiss sources (felsic input) and sediments have undergone intense weathering.

Declarations

Acknowledgements This paper is the result of the second author Master thesis research work at the University of Buea. We gratefully acknowledge the editors for the handling of the manuscript. The authors are grateful to Activation Laboratories (ACTLABS) in Canada for geochemical analysis.

Funding The authors declare that no funds, grants, or other support were received during the preparation of this manuscript.

Competing interests The authors have no relevant financial or non-financial interests to disclose.

Author's contributions All authors contributed to the study conception and design. Material preparation, data collection and analysis were performed by Mbua Elvis Ngomba and Ndema Mbongué Jean-Lavenir. The first draft of the manuscript was written by Mbua Elvis Ngomba and Emmanuel Eseyu Mengu Junior. All authors read and approved the final manuscript.

Data availability statement All data generated or analysed during this study are included in this published article.

Conflict of interest: The authors declare no conflict of interest.

References

1. Alexander, B. W., Bau, M., Andersson, P., Dulski, P. (2008). Continentally-derived solutes in shallow Archean sea water; rare earth element and Nd isotope evidence in iron formation from the 2.9 Ga Pongola Supergroup, South Africa. *Geochimica Cosmochimica Acta*, 72, 378-394.
2. Ali, k., Cheng, Q., Li, W., Chen, Y. (2006). Multi-element analysis of stream sediment geochemistry data for predicting gold deposits in South-Central Yunnan Province, China. *Geochemistry Exploration, Environment, Analysis*, 6, 341-348.
3. Armendariz, V., Herrera, I., Peralta-Videa, J. R., Jose-Yacaman, M., Troiani, H., Santiago, P., Gardea-Torresdey, J. L. (2004). Size control gold nanoparticle formation by *avena sativa* biomass: use of plants in nanobiotechnology. *Journal of Nano Particle Research*, 6, 377-382.

4. Armstrong-Altrin, J. S., Lee, Y. I., Verma, S. P., Ramasamy, S. (2004). Geochemistry of sandstones from the upper Miocene Kudankulam Formation, Southern India: Implications for provenance, weathering, tectonic setting. *Journal of Sedimentary Research*, 74, 285-297
5. Bellehemear, C., Marcotte, D., Jebrak, M. (1994). Multi-element relationship and spatial structures of regional geochemical data from stream sediment, southwestern Quebec. *Canada. Journal of Geochemical Exploration*, 51, 11-35.
6. Bhatia, M. R. (1983). Plate tectonic and geochemical composition of sandstones. *Journal of Geology*, 91, 611-627.
7. Bhatia, M. R., Crook, K. A. (1986). Trace element characteristics of graywackes and tectonic setting discrimination of sedimentary basins. *Contribution to Mineralogy and Petrology*, 92 (2), 181–193.
8. Boyle, R. W. (1984). Gold deposits - an overview of their types, geochemistry, production, and origin. *Geological Survey of Canada, Ottawa*, pp 1 – 13.
9. Boyle, R. W. (1987). Gold. In *General Geochemistry of Gold and Types of Auriferous Deposits. Van Nostrand Reinhold*, Chapter 1, p 2.
10. Castaing, C., Feybesse, J. L., Thiéblemont, D. et al (1994). Palaeogeographical reconstructions of the Pan-African/Brasiliano orogen: closure of an oceanic domain or intracontinental convergence between major blocks? *Precambrian Research*, 69, 327-344. [https://doi.org/10.1016/0301-9268\(94\)90095-7](https://doi.org/10.1016/0301-9268(94)90095-7).
11. Chandrajith, R., Dissanayake, C. B., Tobschall, H. J. (2001). Application of multi-element relationship in stream sediments to mineral exploration: a case study of Walawe Ganga Basin, Sri Lanka. *Applied Geochemistry*, 16, 339-350.
12. Chombong, N. N., Suh, C. E., Ilouga, D. C. (2013). New detrital zircon U-Pb ages from BIF related metasediments in the Ntem Complex (Congo craton) of southern Cameroon, West Africa. *Natural Science Journal*, 5, 835-847.
13. Condie, K. C. (1993). Chemical composition and evolution of the upper continental crust: contrasting results from surface samples and shales. *Chemical Geology*, 104, 1–37.
14. Cullers, R. L., Bock, B., Guidotti, C. (1997). Elemental distribution and neodymium isotopic compositions of Silurian metasediments, western Maine, USA: redistribution of the rare earth elements. *Geochimica Cosmochimica Acta*, 61, 1847–1861.
15. Embui, V. F., Omang, B. O., Che, V. B., Nforba, M. T., Suh, E. C. (2013). Gold grade variation and stream sediment geochemistry of the Vaimba-Lidi drainage system, northern Cameroon. *Natural Science*, 5(2A), 282-290.
16. Etutu, M. E. M. M., Suh, C. E., Vishiti, A., Shemang, E. M., Agyingi, M. C., Mendes, C. J. (2020). Gemstones-bearing sediments in the Mbiame flood plain, northwest Cameroon. *Journal of Sedimentary Environments*. <https://doi.org/10.1007/s43217-00033-4>
17. Floyd, P. A., Leveridge, B. E. (1987). Tectonic environment of the Devonian Gramscatho basin, south Cornwall: framework mode and geochemical evidence from turbiditic sandstones. *Journal of the Geological Society of London*, 144, 531–542
18. Floyd, P. A., Winchester, J. A., Park, R. G. (1989). Geochemistry and tectonic setting of lewisian clastic metasediments from the early Proterozoic loch meree group of gairloch. N W Scotland. *Precambrian Research*, 77, 1191-1212.

19. Fossi, D. H., Dadjo Djomo, H., Takodjou Wambo, J. D., Ganno¹ S., Pour, A. B., Kankeu B., Nzenti, J. P. (2021) Structural lineament mapping in a sub-tropical region using Landsat-8/SRTM data: a case study of Deng-Deng area in Eastern Cameroon. *Arabian Journal of Geosciences*. <https://doi.org/10.1007/s12517-021-08848-9>.
20. Ganwa, A. (1998). Caractérisation géologique d'une unite structural de la deformation tangentielle panafricaine dans la region de Ndom, secteur Kombé Il-Mayabo. Thèse de Doctorat de 3è cycle. Université de Yaoundé, Cameroun.
21. Garret, R. G., Lalor, G. C., Vutchkov, M. (2004). Geochemical exploration for gold in Jamaica: a composition of stream sediment and soil surveys. *Geochemistry: Exploration, Environment, Analysis*, 4, 161-170.
22. Gu, X. X., Liu, J. M., Zheng, M. H., Tang, J. X., Qt, L. (2002). Provenance and Tectonic setting of the Proterozoic turbidites in Hunan, South China: Geochemical Evidence. *Journal of Sedimentary Research*, 72, 393–407.
23. Jahn, B. M., Condie, K. C. (1995). Evolution of the Kaapvaal Craton as viewed from geochemical and Sm-Nd isotopic analyses of intracratonic pelites. *Geochimica Cosmochimica Acta*, 59, 2239–2258. [https://doi.org/10.1016/0016-7037\(95\)00103-7](https://doi.org/10.1016/0016-7037(95)00103-7).
24. Karanlik, S., Aqca, N., Yalcin, M. (2011). Spatial distribution of heavy metals content in soils of Amik plain (Hatay, Turkey). *Environment Monitoring Assessement*, 173, 181–191.
25. Kankeu, B., Greiling, R. O., Nzenti, J. P. et al (2018). Contrasting Pan-African structural styles at the NW margin of the Congo Shield in Cameroon. *Journal of African Earth Science*, 146, 28–47. <https://doi.org/10.1016/j.jafrearsci.2017.06.002>.
26. Kankeu, B., Greiling, R. O., Nzenti, J. P., Bassahak, J., Hell, J. V. (2012). Strain partitioning along the Neoproterozoic Central Africa shear zone system: structures and magnetic fabrics (AMS) from the Meiganga area, Cameroon. *Neues Jahrb Geology of Paleaontolology Abh*, 265, 27-47.
27. Korbel, P., Novak, M. (2001). The complete encyclopedia of minerals. Grange Book PLC, United Kingdom. 296p.
28. Kroonenberg, S. B. (1994). Effects of provenance, sorting and weathering of geochemistry of fluvial sands from different tectonic and climatic environments. In Proc 29th International Geology Congress.
29. Macdonald Eoin, H. (2007). Handbook of gold exploration and evaluation. CRC Press Boca Raton Boston New York Washington, DC, p. 664.
30. Mimba, M. E., Tamnta, N. M., Suh, C. E. (2014). Geochemical dispersion of gold in stream sediments in the paleoproterozoic Nyong series, southern Cameroon. *Science Research*, 2, 155–165.
31. Maynard, J. B., Valloni, R., Shing, H. J. (1982). Composition of modern deep-sea sands from arc-related basin. *Journal of the Geological Society of America*, Special Publication, 10, 551-561.
32. McClenaghan, M. B., Cabri, L. J. (2011). Review of gold and platinum group elements. *Environment Analysis*, 11, 251-263.
33. McLennan, S. M., Hemming, S., McDaniel, D. K. Hanson, G. N. (1993). Geochemical approaches to sedimentation, provenance and tectonics; *Geological Society of America*, Special Papers, 284, 21-40.
34. McQueen, K. G. (2005). Ore deposit types and their primary expressions. CRC LEME, Australian National University, Canberra, ACT 0200 and School of REHS, University of Canberra, ACT 2601. p 1 – 13.

35. Moudioh, C., Soh, T. L., Ganno, S., Nzepang, T. M., Soares, M. B., Ghosh, R., Kankeu, B., Nzenti, J. P. (2020). Tectonic setting of Bipindi greenstone belt, northwest Congo Craton, Cameroon: Implications on BIF deposition. *Journal of African Earth Science*, 171 103971.
36. Neves, S. P., Bruguier, O., Vauchez, A., Bosch, D., Silva, J. M. R., Mariano, G. (2006). Timing of crust formation, deposition of supracrustal sequences, and Transamazonian and Brasiliano metamorphism in the East Pernambuco belt (Borborema Province, NE Brazil): Implications for western Gondwana assembly. *Precambrian Research*, 149(3-4), 197-216.
37. Ndema, M. J. L., Mbonjoh, T. M. (2020). Assessment of Banded Iron Formations around Group Area as Potential High-Grade Iron Ore (Nyoung Series, Congo Craton-South Cameroon). *International Journal of Progressive Sciences and Technologies*, 22(2), 87-110.
38. Ngako, V., Affaton, P., Nnange, J. M., Njanko, T. (2003). Pan-African tectonic evolution in the central and south Cameroon: transpressive and transtension during sinistral shear movements. *Journal of African Earth Science*, 36, 107–214. [https://doi.org/10.1016/S0899-5362\(03\)00023-X](https://doi.org/10.1016/S0899-5362(03)00023-X)
39. Ngatcha, R. B., Okunlola, O. A., Suh, C. E. et al (2019). Petrochemical characterization of Neoproterozoic Colomine granitoids, SE Cameroon: implications for gold mineralization. *Lithos*, 344–345, 175–192.
40. Ngnotue, T., Nzenti, J. P., Barbey, P., Tchoua, F. M. (2000). The Ntui Betamba high grade gneisses: a northward extension of the Pan-African Yaoundé gneisses in Cameroon. *Journal of African Earth Science*, 3(1), 369–381.
41. Nzenti, J. P. (1998). L'Adamaoua panafricain (région de Banyo): une zone clé pour un modèle de la chaîne panafricaine nord- équatoriale au Cameroun. – Thèse Doctorat D'Etat, Université Cheikh Anta Diop (Senegal), Université de Nancy I (France), 176 pp.
42. Nzenti, J. P., Barbey, P., Macaudiere, J., Soba, D. (1988). Origin and evolution of the late Precambrian high grade Yaounde gneisses (Cameroon). *Precambrian Research*, 38, 91-109.
43. Nzenti, J. P., Njanko, T., Tanko Njiosseu, E. L., Tchoua, F. M. (1998). Les domaines granulitiques de la Chaîne Panafricaine Nord–Equatoriale au Cameroun. In Géologie et Environnement au Cameroun, Vicat et Bilong editors, *Collection Geocam I*, 255 –264.
44. Penaye, J., Toteu, S. F., Van Schmus, W. R., Nzenti, J. P. (1993). U-Pb and Sm-Nd preliminary geochronologic data on the Yaoundé series, Cameroon: Re-interpretation of the granulitic rocks as the suture of a collision in the “centrafrican” belt. *Comptes Rendus de l'académie des Science, Paris*, 317, 789–794.
45. Pirajno, F. (1992). Hydrothermal Mineral Deposits. Principles and Fundamental Concepts for the Exploration Geologist (pp. xviii + 709). Berlin, Heidelberg, New York, London, Paris, Tokyo, Hong Kong: Springer-Verlag, [doi:10.1017/S0016756800020392](https://doi.org/10.1017/S0016756800020392).
46. Poidevin, J.L. (1983). La tectonique pan-africaine a la bordure Nord du craton congolais : l'orogenèse des 'Oubanguides'. In: 12th Colloquium of African Geology. Brussels (Abstract).
47. Rodionov, S. M., Obolenskiy, A. A., Dejidmaa, G., Gerel, O., Hwan Hwang, D., Miller, R. J., Nokleberg, W. J., Ogasawara, M., Smelov, A. P., Yan, H., Seminskiy, Z. V. (2013). Descriptions of metallogenic belts, methodology, and definitions, for Northeast Asia mineral deposit location and metallogenic belt maps. UGS, Science for a changing world. p 1- 12.
48. Roser, B. P., Korsch, R. J. (1986). Determination of tectonic setting of sandstone–mudstone suites using SiO₂ content and K₂O/Na₂O ratio. *Journal of Geology*, 94, 635–650.

49. Roser, B. P., Korsch, R. J. (1988). Provenance signatures of sandstones-mudstone suites determine using discrimination function analysis of major-element data. *Chemical Geology*, 67, 119-139.
50. Rudnick, R. L., Gao, S. (2003). Composition of the continental crust. The crust. *Treatise on geochemistry*, 3, 1-64.
51. Soh, T. L., Nzepang, T. M., Chongtaoa, W., Ganno, S, Ngnotue, T., Kouankap Nono G. D., Shaamu, J. S., Zhang, J., Nzenti, J. P. (2018). Geology and geochemical constrains on the origin and depositional setting of the Kpwa-Atog Boga banded iron formations (BIF), northwestern Congo craton southern Cameroon. *Ore Geology Review*, 95, 620-638.
52. Takodjou Wambo, J. D., Pour, A. B., Ganno, S. et al (2020). Identifying high potential zones of gold mineralization in a sub-tropical region using Landsat-8 and ASTER remote sensing data: a case study of the Ngoura-Colomines goldfield, eastern Cameroon. *Ore Geology Review*, 122, 103530. <https://doi.org/10.1016/j.oregeorev.2020.103530>.
53. Taylor, S. R, McLennan, S. M. (1985). The continental crust: its composition and evolution Publishing, Oxford, UK, 312. pp 45-51
54. Taylor, S. R, McLennan S. M. (1995). The geochemical evolution of the continental crust. *Review of Geophysics*, 33, 241–265.
55. Toteu, S. F., Macaudière J, Bertrand JM, Dautel D (1990) Metamorphic zircon s from northern Cameroon: implications for the Pan-African evolution of central Africa. *Geology Rundsch*, 79,777-786.
56. Toteu, S. F., Van Schmus, W. R., Penaye, J., Michard, A. (2001). New U-Pb and Sm-Nd data from North-Central Cameroon and its bearing on the pre-pan African history of Central Africa. *Precambrian Research*, 108, 45-73.
57. Toteu, S. F., Penaye, J., Poudjom, D. Y. (2004). Geodynamic evolution of the Pan-African belt in Central Africa with special reference to Cameroon. *Canadian Journal of Earth Science*, 41, 73-85.
58. Townley, B. K. Herail, G., Maksaev, V., Palacios, C., De Parseval, P., Sepuldeva, F., Orellana, R., Rivas, P., Ulloa, C. (2003). Gold grain morphology and composition as an exploration tool: application to gold exploration in covered areas. *Geochemistry, Exploration, Environment, Analysis*, 3, 29-38.
59. Varga, A., Raucsik, B., Szakmany, G. (2004). On possible origin of Background contents of heavy metals and metalloids in the subsurface Pennsylvania Tenseny metasandstones, SW Hungary.
60. Wedepohl, H. (1995). The composition of the continental crust. *Geochimica Cosmochimica Acta*, 59, 1217-1239.
61. William, M. H. (2016). CRC Handbook of Chemistry and Physics, vol. 97, CRC Press/Taylor and Francis, 2652 p. (ISBN 1498754287), « Abundance of elements in the Earth's crust and in the sea », 2402, 14-17.
62. Yang, X., Liu, L., Lee, I., Wang, B., Du, Z., Wang, Q., Wang. Y., Sun, W. (2014). A review on the Huoqiu banded iron formation (BIF), southeast margin of the North China Craton: genesis of iron deposits and implications for exploration. *Ore Geology Review*, 63, 418–443. <https://doi.org/10.1016/j. Ore Geology Review, 2014.04.002>.
63. Youngson, J., Craw, D. (1999). Variation in Placer Style, Gold Morphology, and Gold Particle Behaviors Down Gravel Bed-Load Rivers : An Example from the Shotover/Arrow-Kawarau-Clutha River System, Otago, New Zealand. *Economic Geology*, 94, 615-634.

Figures

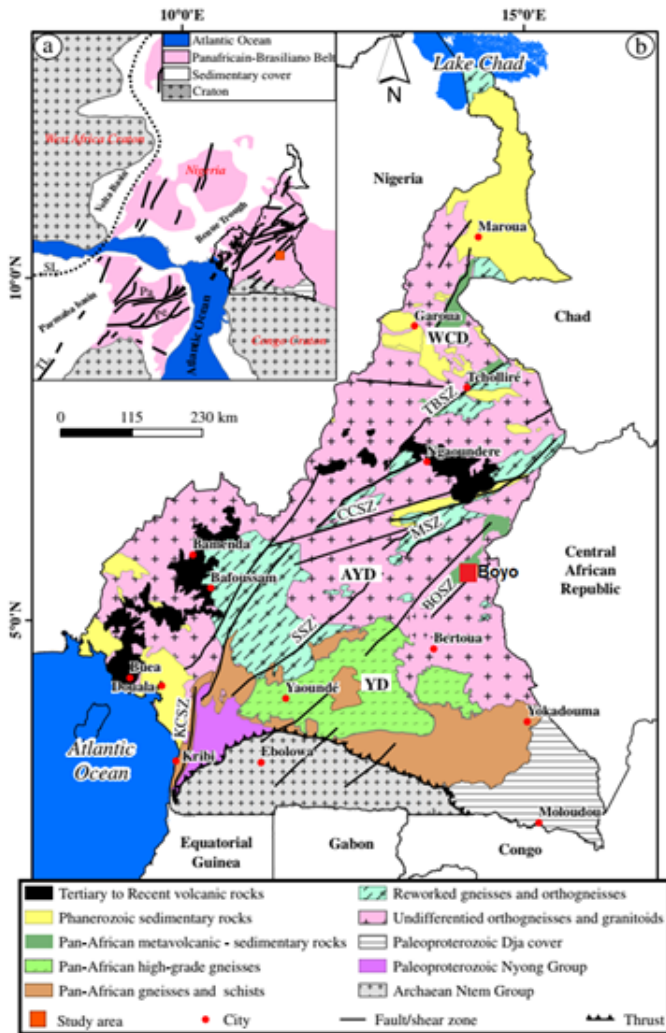


Figure 1

(a) Reconstitution map of the Pan-African NE Brazilian and West African domains showing the continuity between the Sergipano and North Equatorial ranges (after Castaing et al. 1994). (b) Geologic map of Cameroon (Kankeu et al. 2018; Fossi et al., 2021) showing the location of the Boyo area and the main lithotectonic domains. YD: Yaounde domain; AYD: Adamawa Yade domain; WCD: Western Cameroon domain; BOSZ: Bétare-Oya Shear Zone; SSZ: Sanaga Shear Zone; Pe: Permambuco Shear Zone; Pa: Patos Shear Zone TBSZ: Tibati-Banyo Shear Zone; SL: Suture Line; KF: Kandi Fault; KCSZ: Kribi-Campo Shear Zone; NT: Ntem complex; DS: Dja Series; NS: Nyong Complex

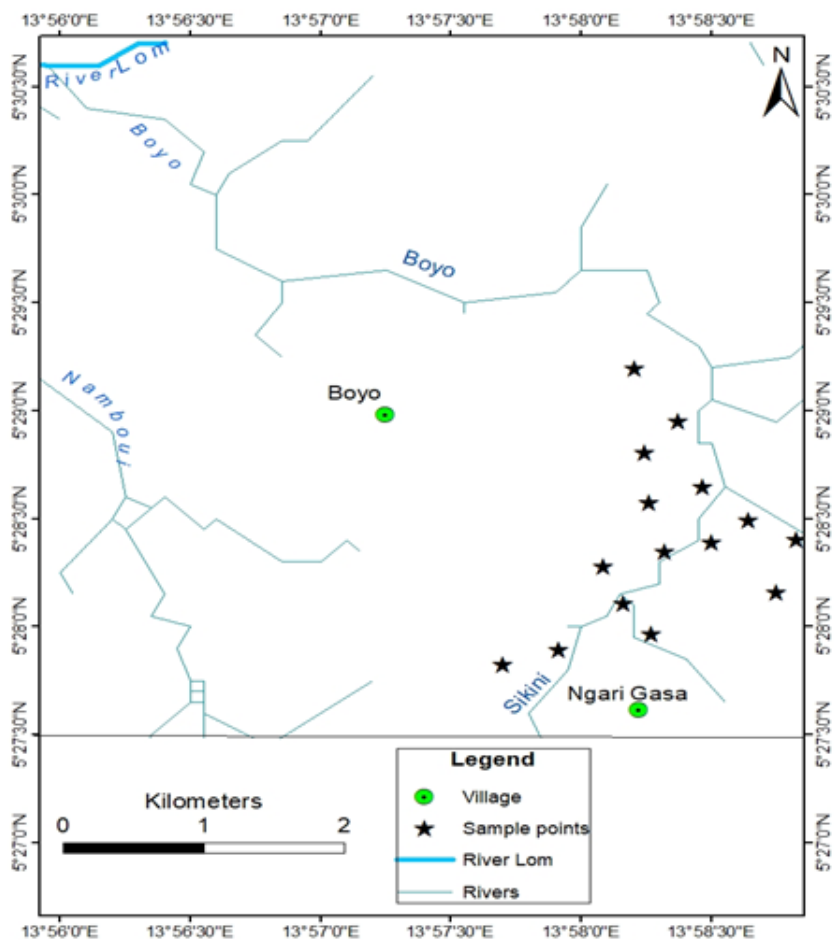


Figure 2

Sample location map of the study area

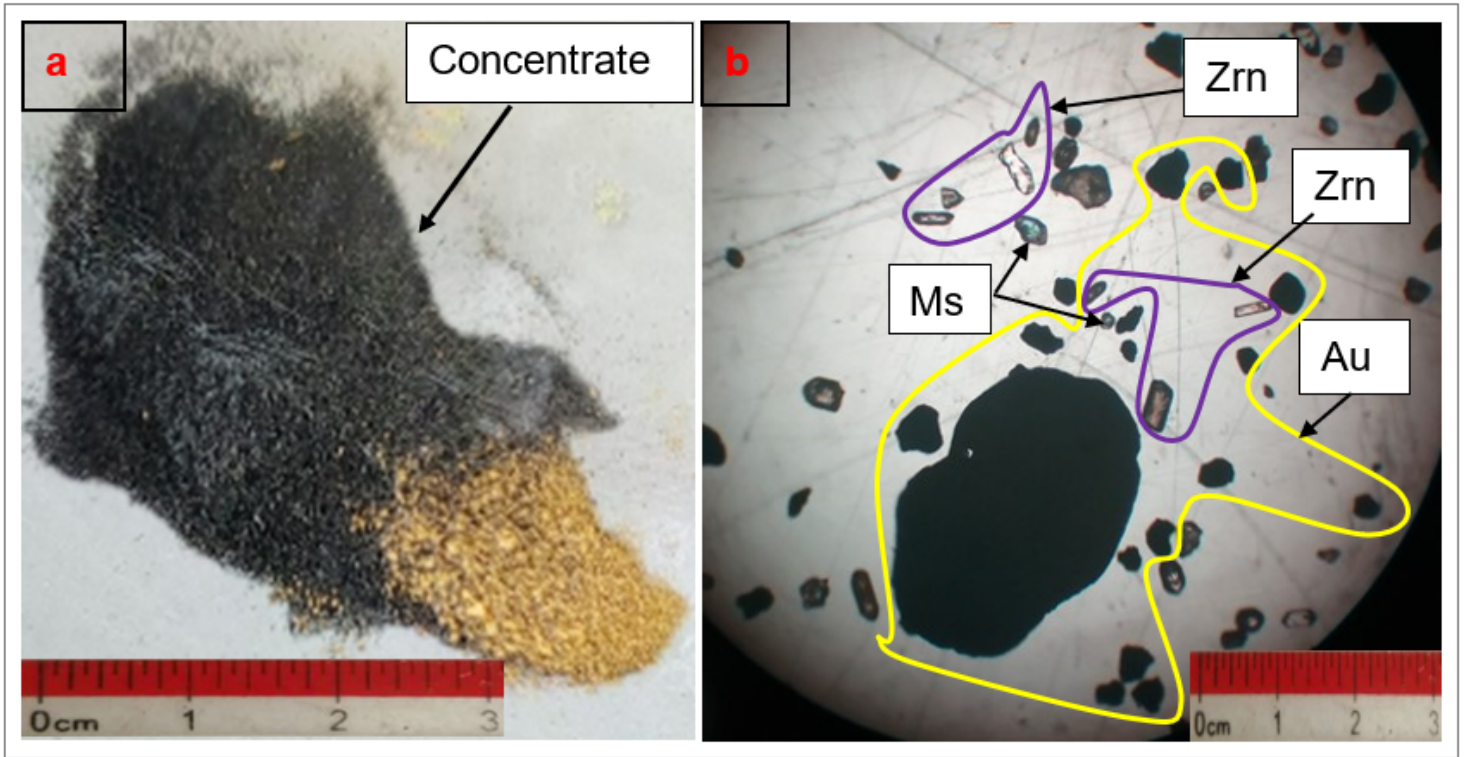


Figure 3

(a) Heavy mineral concentrate showing a lot quantity of gold grains. (a) Photomicrograph of mineral grains in stream sediment from Boyo area. Zrn = zircon, Au = gold, Ms = muscovite

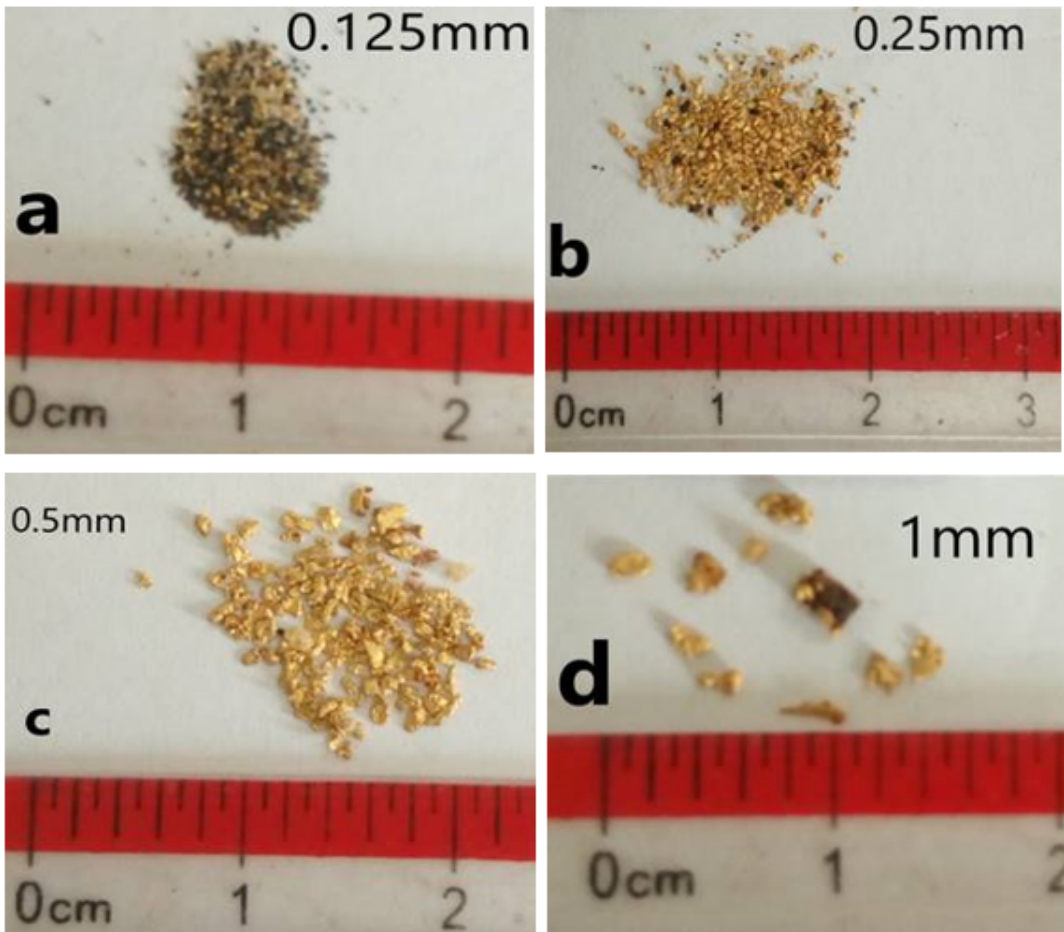


Figure 4

Gold grains recovered from stream sediments in Boyo display various outlines and morphologies. Note the particle sizes: (a) 0.125 mm, (b) 0.25 mm, (c): 0.5 mm, (d): 1 mm

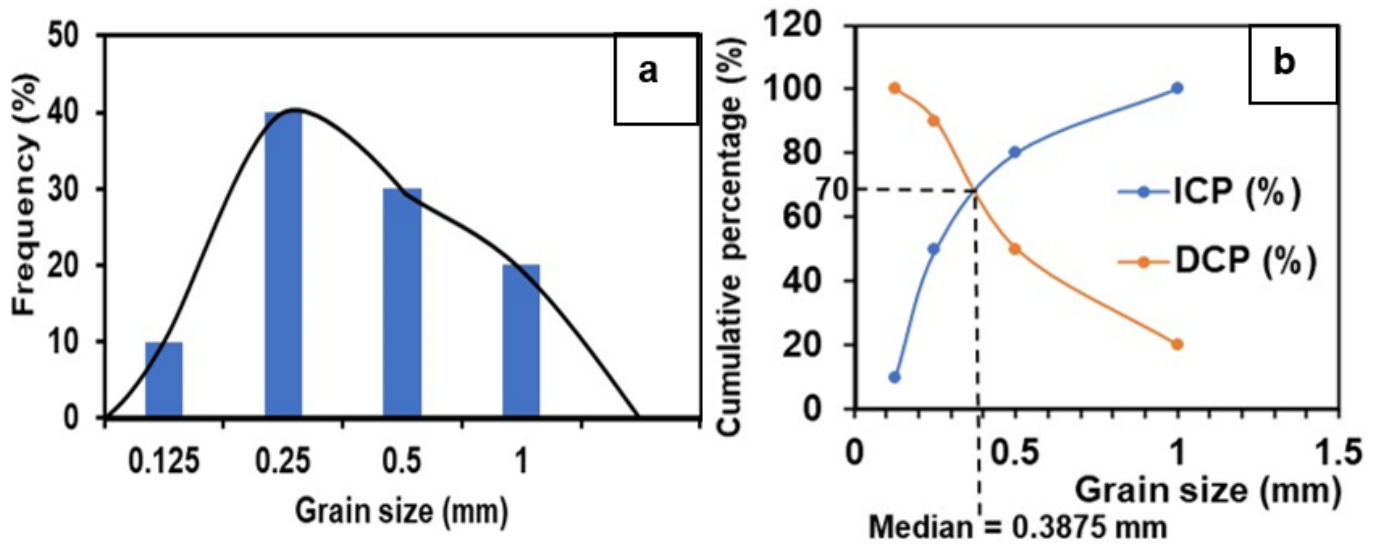


Figure 5

Grain size distribution of gold in stream sediment. (a) Bar chart representation and (b) cumulative percentage curves showing the median value (median = 0.3875 mm). ICP: increase cumulative percentage, DCP: decrease cumulative percentage

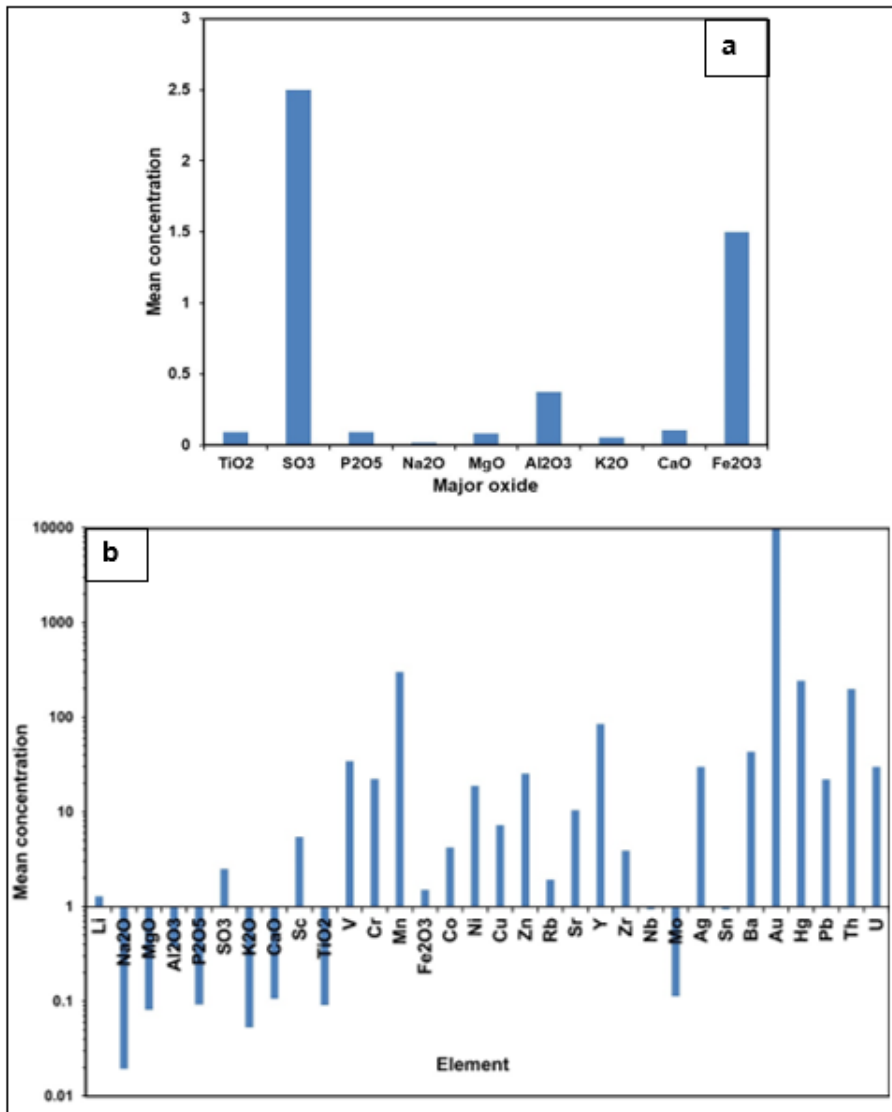


Figure 6

(a) Major elements occurrence in stream sediments. (b) Enrichment-depletion diagram for major and trace elements

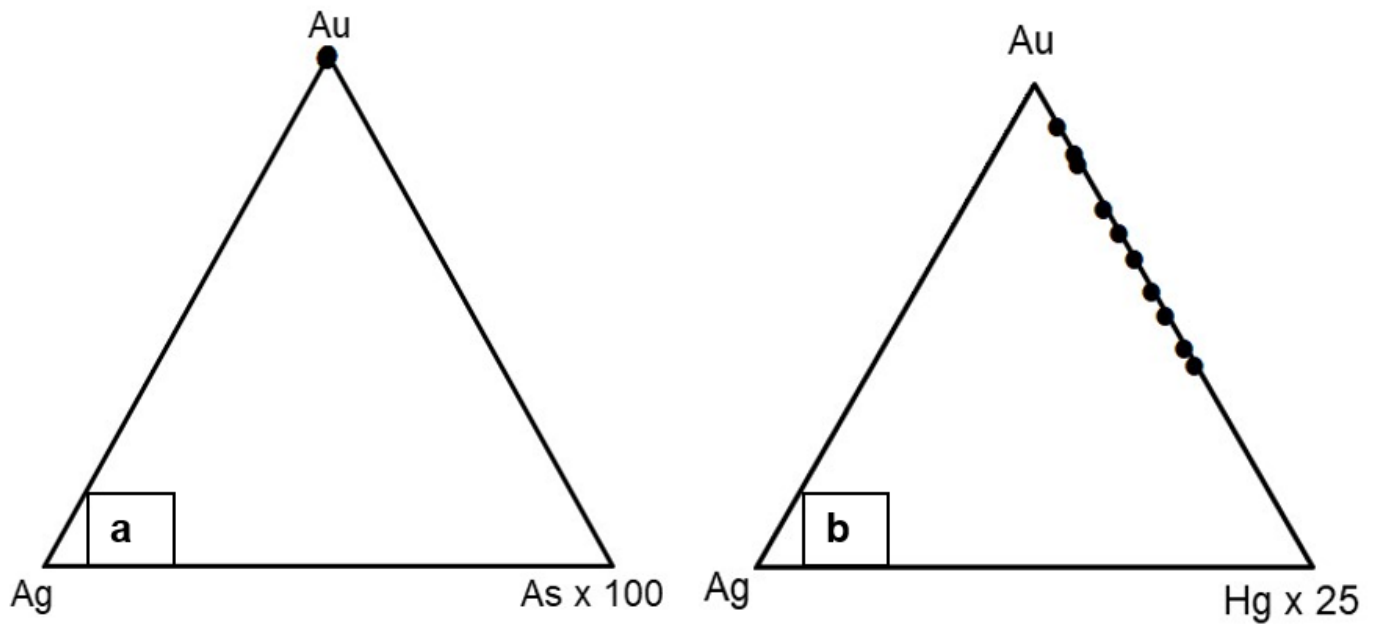


Figure 7

(a) Ternary plots of (a) Au–Ag–As and (b) Au–Ag–Hg respectively showing very high content of Au, low content of As and low to moderate concentration of Hg in stream sediment from Boyo.

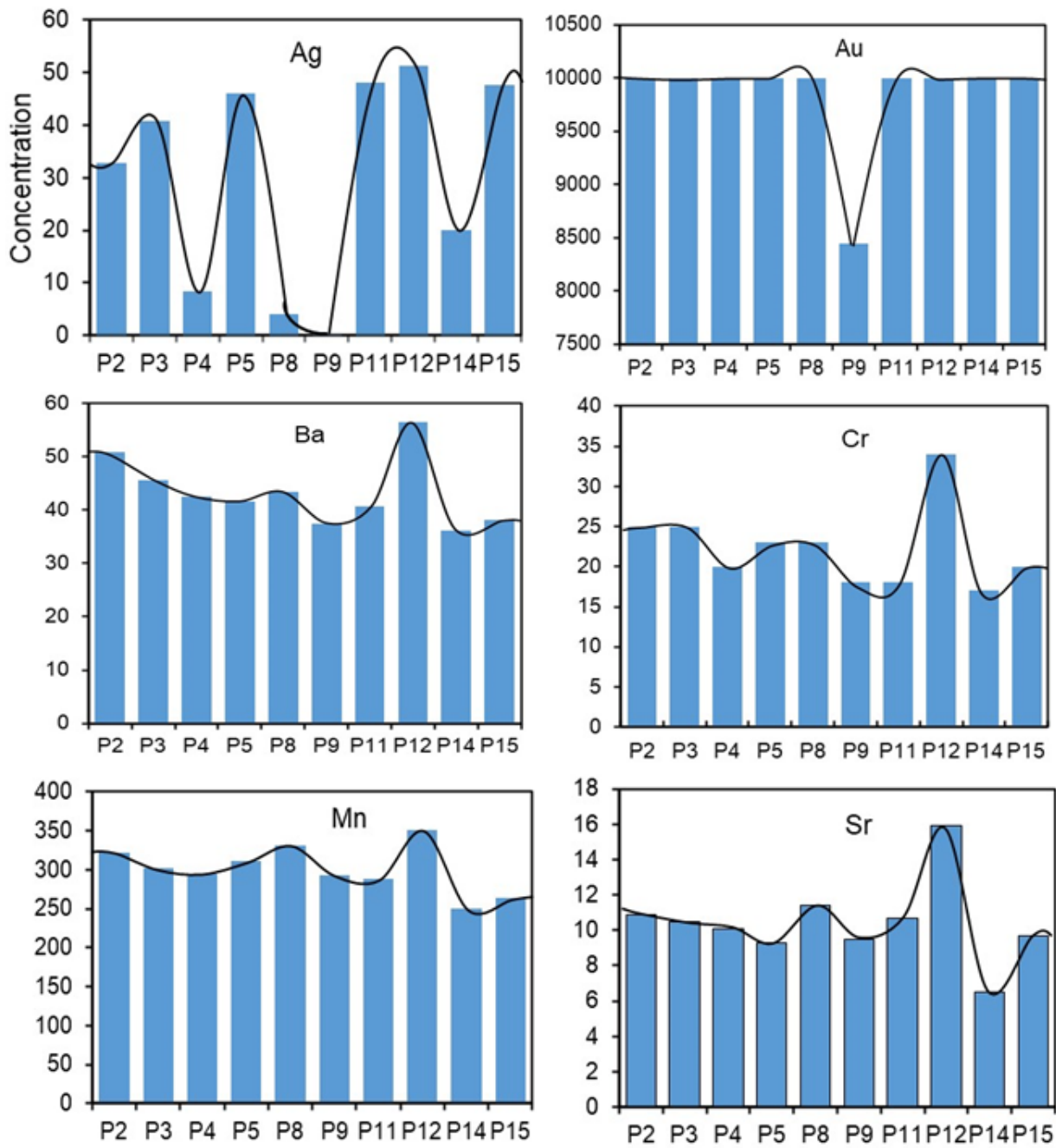


Figure 8

Frequency bar chart for some selected trace elements showing normal and symmetric distribution

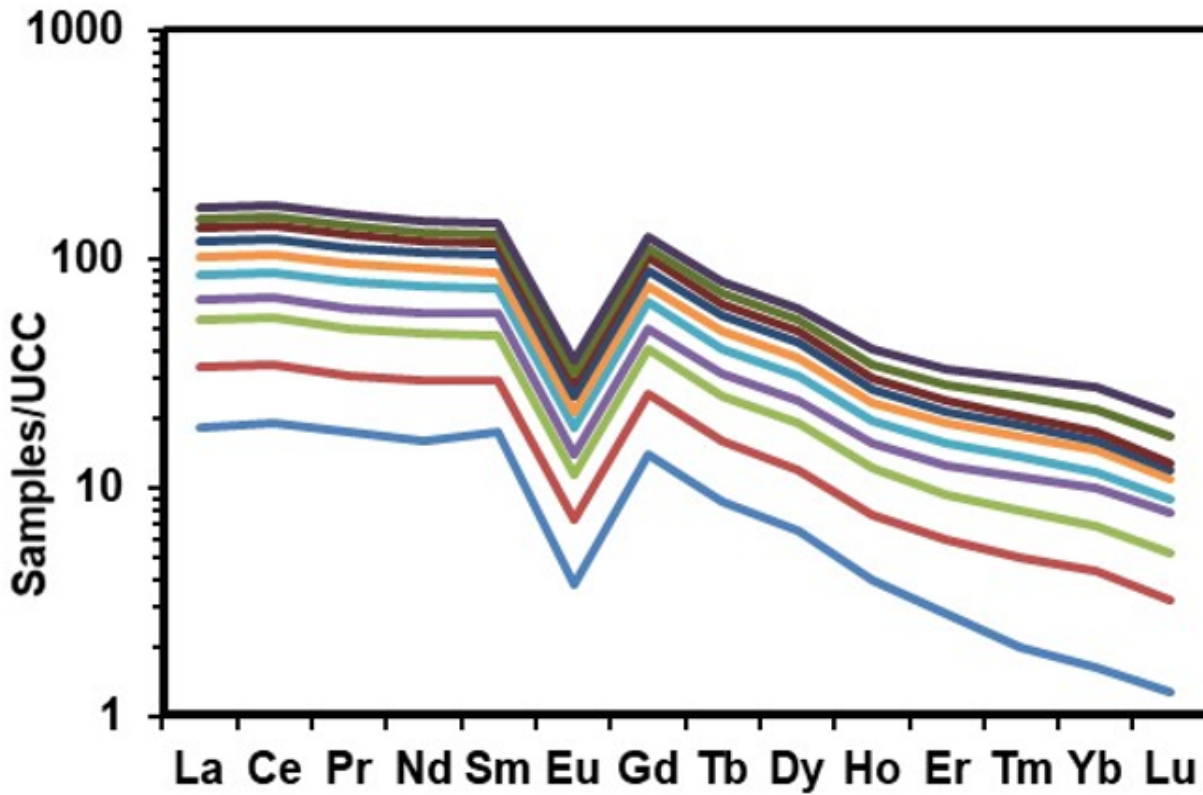


Figure 9

Upper continental crust pattern normalized rare earth elements. Normalization values are according to Rudnick and Gao (2003)

	TiO ₂	Fe ₂ O ₃	Al ₂ O ₃	MgO	CaO	K ₂ O	Na ₂ O	P ₂ O ₅	Ag	Au	B	Ba	Be	Bi	Co	Cr	Cs	Cu	Hf	Hg	Mn	Mo	Nb	Ni	Pb	Rb	Re	Sb	Sc	Sn	Sr	Th	U	V	Y	Zn	Zr			
TiO ₂	1																																							
Fe ₂ O ₃	-0.09	1																																						
Al ₂ O ₃	0.66	-0.37	1																																					
MgO	-0.19	-0.20	0.15	1																																				
CaO	0.47	0.57	0.88	0.25	1																																			
K ₂ O	-0.14	-0.58	0.43	0.45	0.74	1																																		
Na ₂ O	-0.09	0.87	-0.27	-0.25	0.55	0.54	1																																	
P ₂ O ₅	0.66	-0.37	0.60	0.37	0.42	-0.02	-0.38	1																																
Ag	0.29	-0.17	0.50	0.35	0.18	-0.10	-0.04	0.67	1																															
Au	0.08	0.27	0.24	0.16	0.08	0.09	0.28	0.03	0.52	1																														
B	0.31	-0.58	0.23	0.19	0.39	0.49	-0.46	0.14	-0.23	-0.27	1																													
Ba	0.63	-0.23	0.92	0.11	0.85	0.42	-0.21	0.56	0.37	0.33	0.08	1																												
Be	-0.24	0.15	-0.50	-0.69	-0.63	-0.63	0.22	-0.37	0.01	0.00	-0.41	0.55	1																											
Bi	0.20	0.60	-0.16	0.11	-0.42	-0.64	0.54	0.21	0.41	0.49	-0.45	-0.02	0.14	1																										
Co	0.74	-0.23	0.96	0.06	0.81	0.28	-0.24	0.68	0.48	0.23	0.05	0.94	-0.46	-0.05	1																									
Cr	0.77	-0.25	0.95	-0.05	0.82	0.29	-0.24	0.57	0.43	0.30	0.09	0.94	-0.37	-0.06	0.98	1																								
Cs	0.37	-0.39	0.72	0.42	0.91	0.80	-0.42	0.29	-0.02	0.09	0.48	0.77	-0.85	-0.32	0.85	0.84	1																							
Cu	0.46	-0.02	0.48	0.22	0.49	0.33	-0.20	0.27	0.27	0.71	0.16	0.59	-0.37	0.27	0.50	0.58	0.55	1																						
Hf	-0.33	-0.13	-0.18	-0.12	0.15	0.33	-0.28	-0.43	-0.29	0.27	-0.17	0.06	0.14	-0.06	-0.15	-0.05	0.18	0.37	1																					
Hg	-0.26	-0.22	0.14	0.22	-0.03	0.04	0.06	0.02	0.67	0.36	-0.12	-0.12	0.31	0.07	-0.02	-0.01	-0.23	-0.10	-0.14	1																				
Mn	0.74	-0.33	0.81	0.16	0.87	0.48	-0.39	0.48	0.09	0.09	0.46	0.84	-0.66	-0.12	0.81	0.82	0.88	0.65	0.06	-0.30	1																			
Mo	0.42	-0.31	0.83	0.19	0.93	0.62	-0.38	0.30	0.14	0.15	0.12	0.87	-0.61	-0.28	0.84	0.83	0.87	0.53	0.23	-0.11	0.85	1																		
Nb	0.35	-0.61	0.81	0.33	0.95	0.78	-0.52	0.43	0.14	-0.06	0.43	0.79	-0.72	-0.50	0.72	0.69	0.89	0.28	0.03	-0.06	0.76	0.84	1																	
Ni	0.31	0.11	0.37	0.12	0.47	0.26	-0.11	0.29	-0.06	0.21	-0.20	0.69	-0.54	0.14	0.52	0.49	0.57	0.50	0.37	-0.61	0.55	0.60	0.45	1																
Pb	0.22	0.22	-0.18	-0.09	-0.06	-0.21	0.10	0.11	-0.40	-0.37	0.09	0.06	-0.35	0.35	-0.08	-0.13	0.18	-0.04	0.07	-0.66	0.25	0.00	0.01	0.46	1															
Rb	0.24	-0.60	0.62	0.43	0.87	0.68	-0.56	0.27	-0.10	-0.13	0.65	0.61	-0.81	-0.56	0.50	0.48	0.93	0.32	0.08	-0.19	0.75	0.73	0.93	0.39	0.11	1														
Re	0.32	0.00	0.54	0.02	0.66	0.53	-0.20	0.10	0.13	0.33	0.00	0.75	0.54	-0.19	0.62	0.65	0.73	0.67	0.41	-0.48	0.68	0.78	0.58	0.84	0.07	0.58	1													
Sb	0.19	0.40	0.13	0.22	0.10	-0.19	0.16	0.32	0.16	0.21	-0.59	0.43	-0.32	0.58	0.34	0.25	0.20	0.30	0.22	-0.40	0.26	0.32	0.07	0.80	-0.59	-0.04	0.43	1												
Sc	-0.30	0.30	-0.52	-0.52	-0.72	-0.70	0.33	-0.32	0.10	0.02	-0.54	-0.60	0.95	0.20	-0.46	-0.41	-0.92	-0.43	-0.05	0.35	-0.76	-0.66	-0.78	-0.57	-0.41	-0.90	-0.58	-0.27	1											
Sn	0.07	0.31	0.01	0.28	0.18	0.19	0.21	-0.07	-0.27	0.23	-0.02	0.33	0.54	0.38	0.06	0.05	0.48	0.40	0.42	-0.50	0.37	0.28	0.19	0.71	0.72	0.30	0.49	0.67	-0.61	1										
Sr	0.52	-0.59	0.94	0.23	0.98	0.69	-0.51	0.49	0.34	0.14	0.39	0.86	-0.57	-0.39	0.86	0.86	0.84	0.48	0.03	0.11	0.84	0.89	0.93	0.37	-0.18	0.81	0.59	0.02	-0.84	0.05	1									
Th	-0.66	-0.03	0.03	0.09	0.24	0.53	0.01	-0.43	-0.28	-0.11	-0.27	0.09	-0.22	-0.54	0.00	-0.05	0.26	-0.29	0.27	0.03	-0.12	0.34	0.37	0.22	-0.20	0.32	0.33	0.04	-0.17	0.11	0.17	1								
U	-0.36	-0.21	-0.04	0.23	0.40	0.71	-0.35	-0.37	-0.63	-0.02	0.15	0.18	-0.44	-0.39	-0.06	-0.04	0.59	0.25	0.74	-0.39	0.28	0.44	0.42	0.83	0.26	0.58	0.59	0.21	-0.57	0.60	0.24	0.59	1							
V	0.59	-0.29	0.92	-0.10	0.83	0.35	-0.27	0.45	0.35	0.15	-0.02	0.86	-0.31	-0.26	0.94	0.95	0.61	0.37	-0.02	0.04	0.72	0.87	0.73	0.44	-0.22	0.49	0.63	0.20	-0.33	-0.06	0.86	0.21	0.04	1						
Y	-0.63	0.09	-0.62	-0.50	-0.52	-0.27	0.03	-0.63	-0.24	-0.01	-0.49	-0.58	0.82	-0.10	-0.58	-0.50	-0.68	-0.32	0.52	0.19	-0.68	-0.43	0.59	-0.33	-0.35	-0.61	-0.28	-0.22	0.77	-0.35	-0.54	0.21	0.07	-0.35	1					
Zn	0.90	-0.02	0.70	-0.09	0.47	-0.19	-0.04	0.66	0.49	0.29	0.02	0.73	-0.17	0.44	0.78	0.80	0.35	0.56	-0.12	-0.08	0.71	0.50	0.30	0.40	0.22	0.12	0.34	0.44	-0.23	0.18	0.51	-0.63	-0.31	0.63	-0.50	1				
Zr	0.41	-0.63	0.81	0.39	0.95	0.81	-0.53	0.41	0.20	0.12	0.57	0.77	-0.71	-0.38	0.69	0.69	0.93	0.50	0.11	0.04	0.84	0.81	0.94	0.38	-0.02	0.92	0.56	0.00	-0.81	0.25	0.94	0.16	0.42	0.66	-0.62	0.39	1			

Key
 Moderate correlation (r = 0.5 - 0.69)
 Strong correlation (r = 0.70 - 0.79)
 Very strong correlation (r = 0.80 - 0.99)

Figure 10

Pearson's correlation matrix

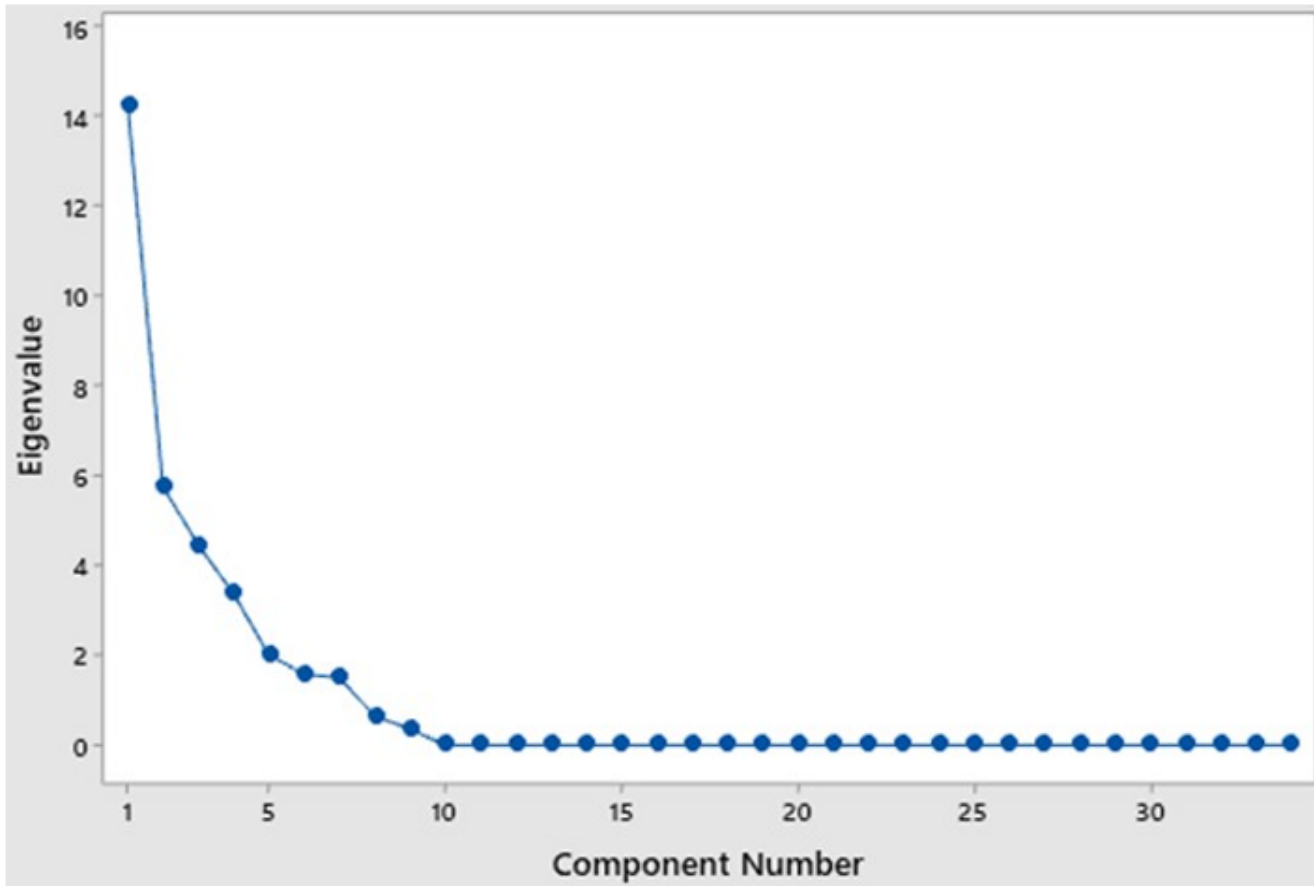


Figure 11

The scree plot showing the calculated eigenvalues arranged from the largest to the smallest values

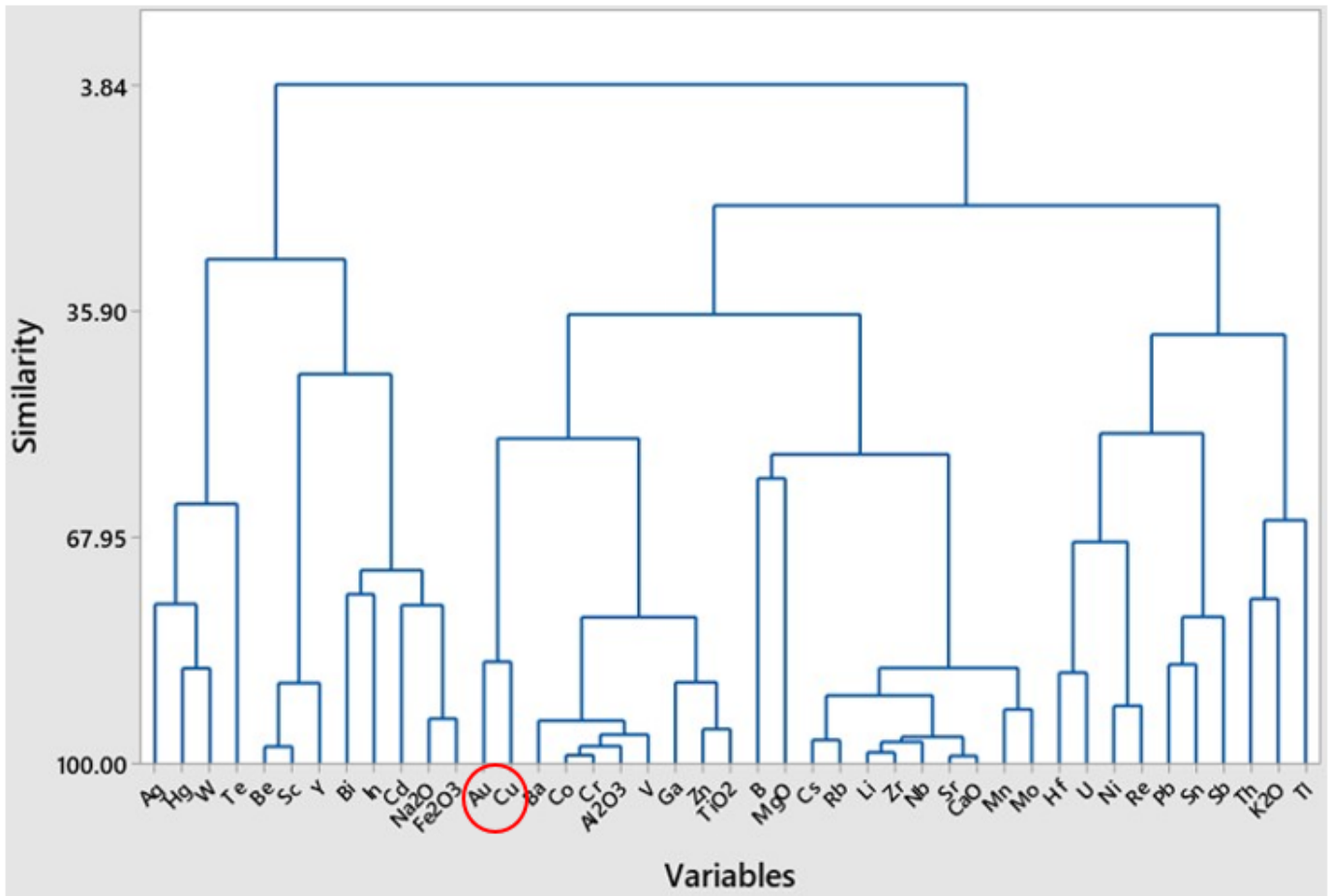


Figure 12

Dendrogram from cluster analysis

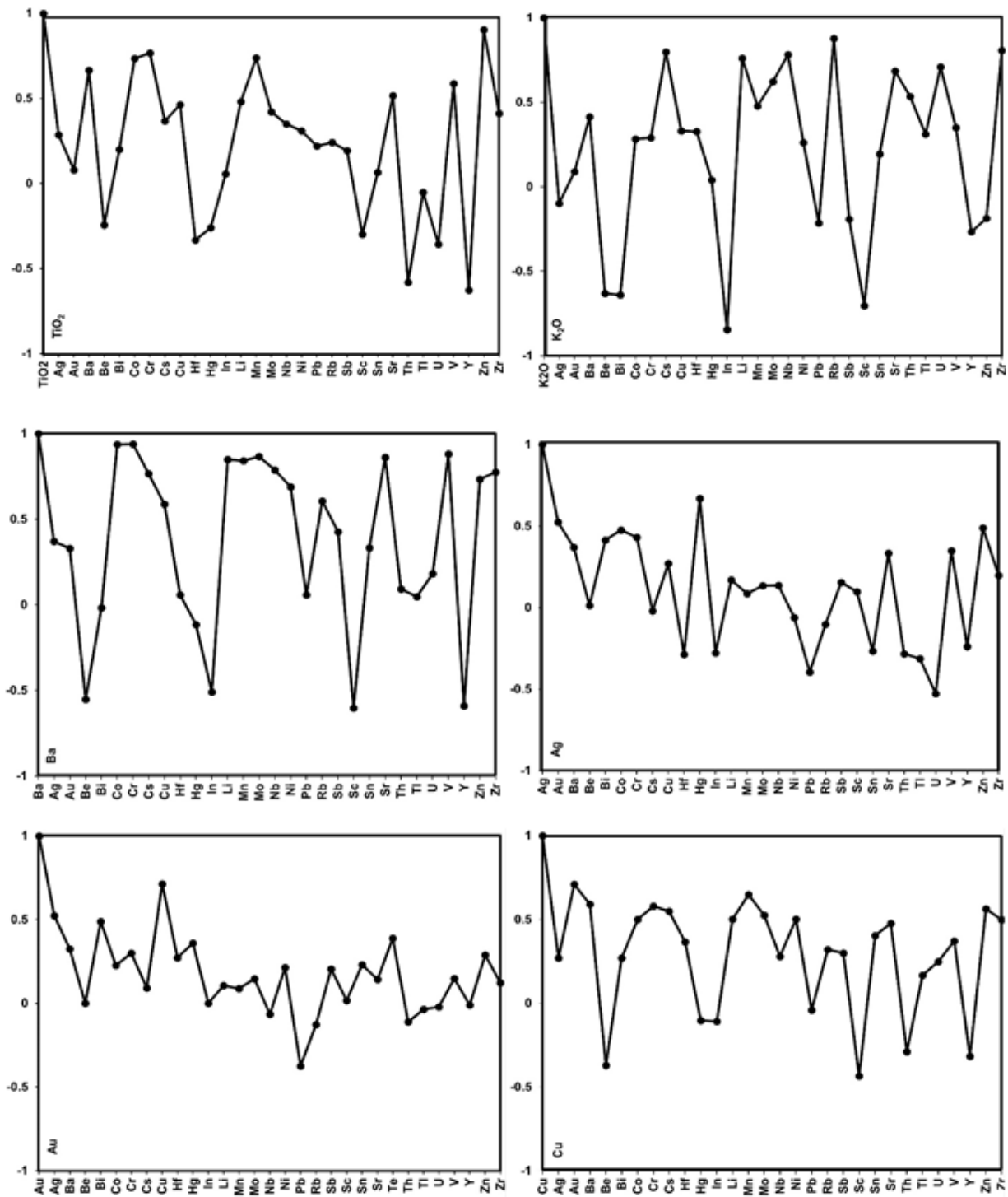


Figure 13

Selected correlation coefficient patterns for TiO₂, K₂O, Ba, Ag, Au and Cu for the studied stream sediment samples from Boyo

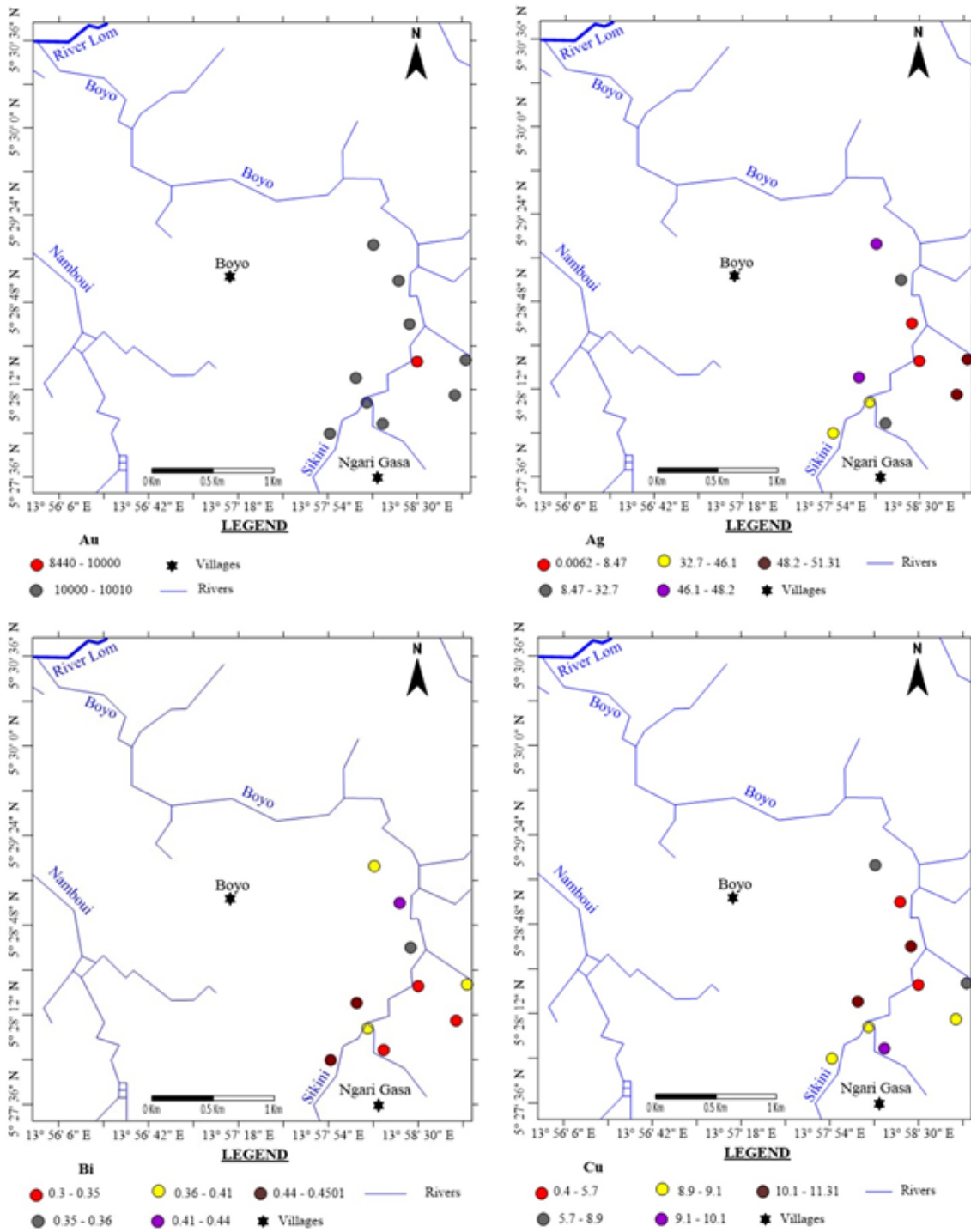


Figure 14

Geochemical distribution map of Ag, Au, Bi and Cu

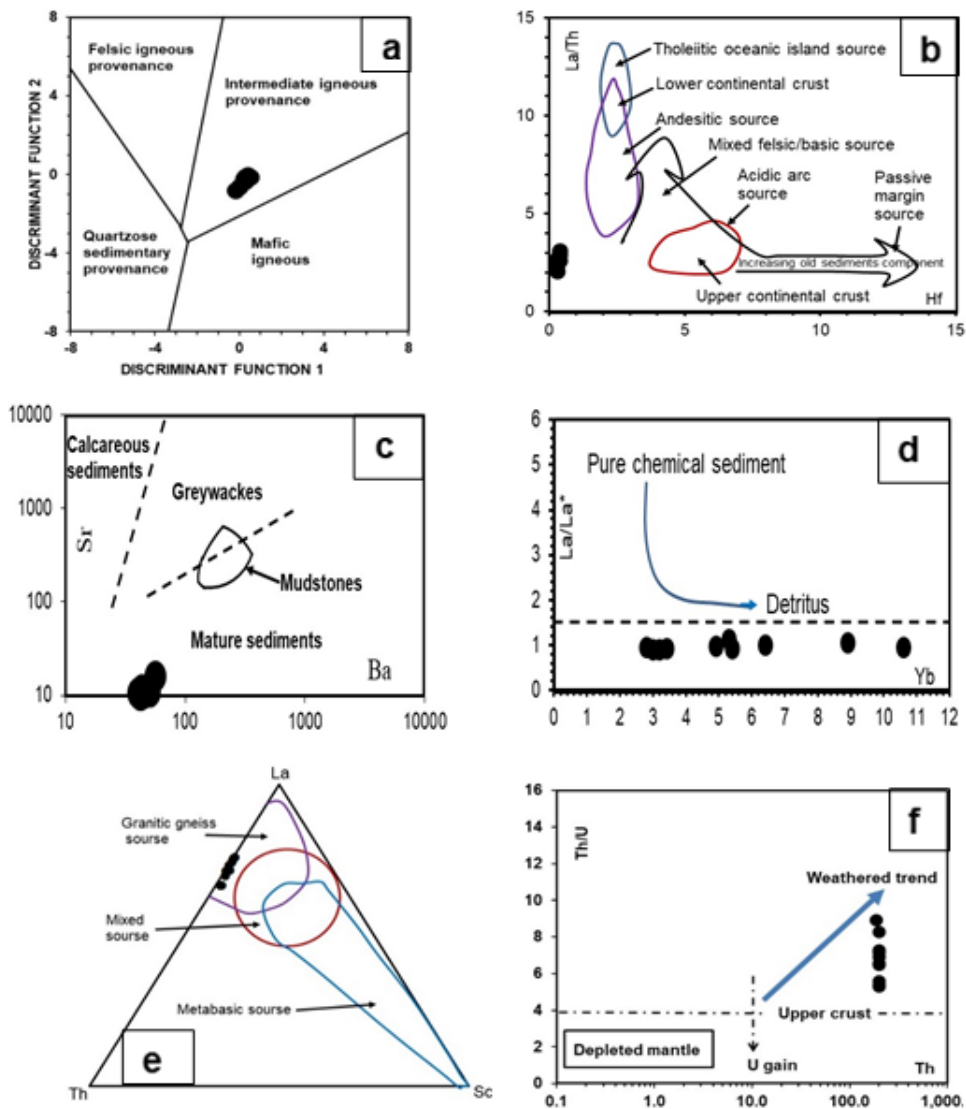


Figure 15

(a) Discriminant function diagram (Roser and Korsch, 1988) of major elements. The discriminant functions are: Discriminant Function 1 = $-1.773\text{TiO}_2 + 0.607\text{Al}_2\text{O}_3 + 0.76\text{Fe}_2\text{O}_3(\text{total}) - 1.5\text{MgO} + 0.616\text{CaO} + 0.509\text{Na}_2\text{O} - 1.224\text{K}_2\text{O} - 9.09$. Discriminant Function 2 = $0.445\text{TiO}_2 + 0.07\text{Al}_2\text{O}_3 - 0.25\text{Fe}_2\text{O}_3(\text{total}) - 1.142\text{MgO} + 0.438\text{CaO} + 1.475\text{Na}_2\text{O} + 1.426\text{K}_2\text{O} - 6.861$. (b) Discriminative plot for the provenance of the Boyo sediments La/Th vs. Hf modified after Floyd and Leveridge (1987) and Cullers (1994) respectively. Mean reference contents are from Condie (1993). (c) Plot of Sr vs. Ba diagram for stream sediments from Boyo after Floyd et al. (1989). (d) Yb v. (La/La*) diagram of Alexander et al. (2008) show the chemical nature of the sediments at Boyo. (e) La-Th-Sc ternary plot (Bhatia and Crook 1986) to assess the source of detrital contamination in stream sediments from Boyo. (f) Th/U vs. Th adopted from McLennan et al. (1993). Fields and trends from Gu et al. (2002). Th/U ratios higher than the upper crust value follow the weathering trend

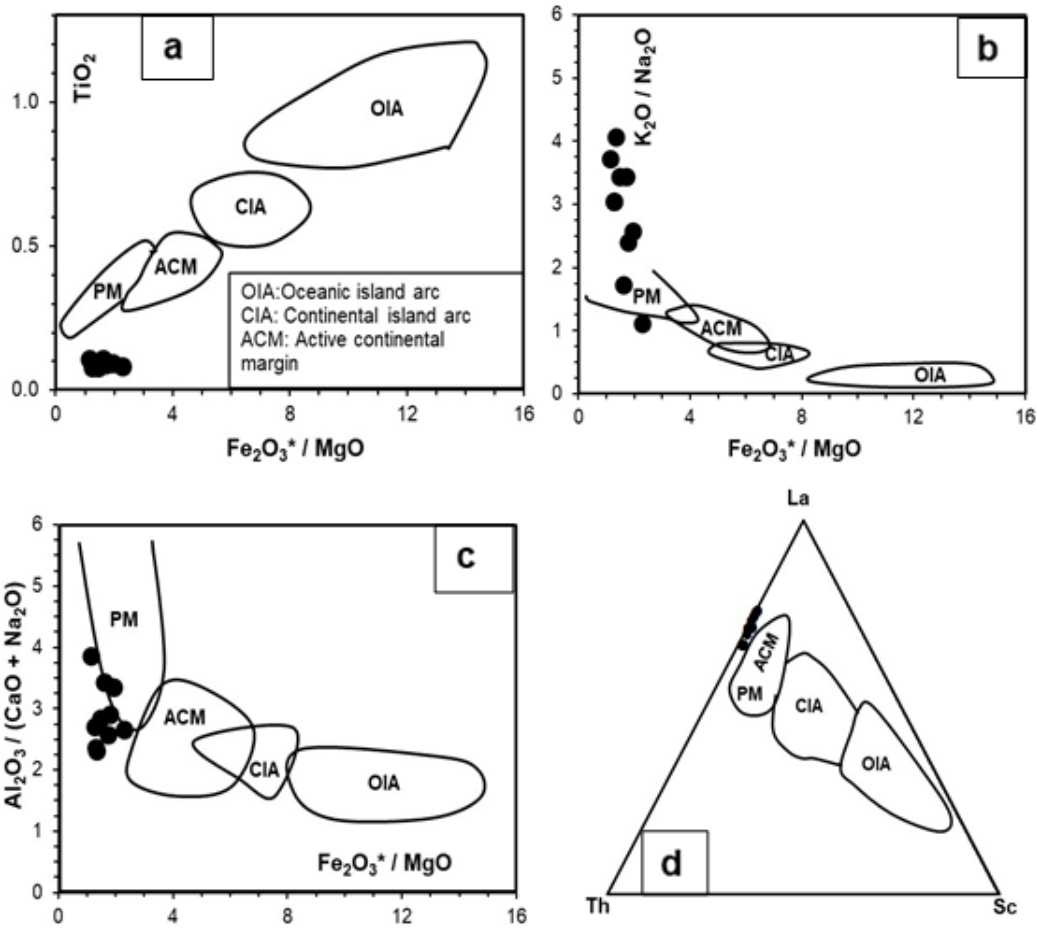


Figure 16

Evaluation of discrimination diagrams of tectonic settings for the Boyo stream sediment samples based upon the bivariate plots (Bhatia, 1983) (a): $Fe_2O_3^* + MgO - TiO_2$; (b): $Fe_2O_3^* + MgO - K_2O/Na_2O$; (c): $Fe_2O_3^* + MgO - Al_2O_3 / (CaO + Na_2O)$; $Fe_2O_3^*$ represents total Fe expressed as Fe_2O_3 . (d): a ternary plot La - Th - Sc (Roser and Korsch, 1986)